Metabolomic fingerprinting in glomerular disease-associated renal amyloidosis

Shreya Ghosh[1,2], Praveen Singh[3,4], Samir Govil[5], Ashok Verma[6], Chayanika Kala[7], Shivani Chitkara[3], Shantanu Sengupta[3,4], Ashwani Kumar Thakur[1,2*]

[1]Department of Biological Sciences and Bioengineering, Indian Institute of Technology Kanpur, Uttar Pradesh-208016, India.

[2]Mehta Family Centre for Engineering in Medicine, Indian Institute of Technology Kanpur, Uttar Pradesh-208016, India.

[3]CSIR-Institute of Genomics and Integrative Biology, New Delhi, India.

[4]Academy of Scientific and Innovative Research (AcSIR), Ghaziabad, India.

[5]Department of Medicine, GSVM Medical College Kanpur, Uttar Pradesh-208019, India.

[6]Department of Radiology, GSVM Medical College Kanpur, Uttar Pradesh-208019, India.

[7]Department of Pathology, GSVM Medical College Kanpur, Uttar Pradesh-208019, India.

*Corresponding author: Dr. Ashwani K Thakur, Department of Biological Sciences and Bioengineering, Mehta Family Centre for Engineering in Medicine, Indian Institute of Technology Kanpur, Uttar Pradesh-208016, India. **E-mail:** akthakur@iitk.ac.in.

Abstract

Background

Minimal change disease (MCD), a glomerular disease subtype is characterised by no visible change in the glomerulus upon light microscopy except for the urinary excretion of excess proteins. The symptoms of minimal change disease and renal amyloidosis are mostly overlapping and thereby misdiagnosed. However, the possible linkage between these two disease types has not been documented. We hypothesised that amyloid formation could be one of the players promoting the pathology associated with minimal change disease, resulting in perturbations of the downstream cellular pathways.

Methods

One hundred glomerular diseased patients were identified in a two-year study, based on symptoms and biochemical markers. Histopathological analysis showed predominance of minimal change disease in twenty patients. Further, gold standard Congo red staining was performed in these patients to detect amyloid deposition followed by tracking its downstream effects on cellular pathways using mass-spectrometry-based untargeted approach.

Results

Congo red staining showed presence of amyloid deposits in eleven minimal change diseased patients. Further, plasma metabolomic fingerprinting revealed a total of fifteen biologically important metabolites altered in minimal change diseased patients having renal amyloidosis as compared to controls. Different classes of lipids, carnitines and amino acids were found to be dysregulated in these patients.

Conclusion

In the present study we have shown the onset of renal amyloidosis and associated pathogenesis in minimal change diseased patients. Additionally, we have identified novel altered metabolic signatures in these patients as compared to controls. This is the first study in context to the Indian population, depicting the potential of metabolomic fingerprinting to identify novel markers for early diagnosis of amyloid formation in minimal change disease, a glomerular disease type.

Keywords minimal change disease, amyloid, renal, metabolomics, untargeted, mass spectrometry

1. Introduction

Glomerulus, the filtering unit of kidney is built up of a bunch of capillaries and four types of specialized differentiating cells namely podocytes, mesangial cells, endothelial cells and parietal epithelial cells [1]. Any sort of damage posed to the glomerulus often leads to the onset of a class of heterogeneous kidney disorders termed as glomerular diseases. Primarily, glomerular disease can be caused either by membranous inflammation, infection or drug toxicity of kidney. However, other disease conditions like diabetes mellitus, systemic lupus erythromatosus, endocarditis, rheumatoid arthiritis and scleroderma often causes glomerular dysfunction, progressing to secondary glomerular diseases [2].

The epidemiology of glomerular disease widely varies among countries and even amongst the individuals of similar race/ ethnicity [3]. In a 30-year cross sectional observational study carried out in south-eastern US, a diverse trend in prevalence rate of glomerular disease subtypes was noted. One of the glomerular disease subtypes, focal segmental glomerulosclerosis (FSGS) was found predominant during the entire study period (1986-2015). But increased frequency of other subtypes, lupus and membranous nephropathy was observed in the middle phase of the study (1996-2005). Diabetic glomerulosclerosis was the most prevalent glomerular disease subtype in the recent times (2006-2015) [4]. Another kidney biopsy-based study conducted in four different continents also depicted varying frequency of glomerular diseases subtypes across different regions. Predominance of diabetic glomerulosclerosis and focal segmental glomerulosclerosis (FSGS) was observed in North America. Lupus nephritis was observed to be highly prevalent in Latin America. Whereas IgA nephropathy was more prevalent in Asia and less prevalent in Europe. Diabetic glomerulosclerosis was highly prevalent in Europe [3]. Similarly, a US-based study observed variations in the frequency of FSGS and not for the other glomerular subtypes. Lupus nephritis is the most common form of secondary glomerular disease observed in Indian population [5]. However, various population-based studies have documented minimal change disease (MCD), IgA nephropathy, membranous nephropathy and focal segmental glomerulosclerosis as the most prevalent form of primary glomerular disease subtypes in India [5-10].

Glomerular diseases are a diagnostic dilemma as the clinical manifestations varies among different subtypes [11]. One of its subtypes, minimal change disease accounts for 15% of the adult patients with idiopathic nephrotic syndrome [12]. Proteinuria, edema and hypoalbuminemia are the primary symptoms observed in these patients [12, 13]. The

diagnosis of MCD is often challenging for the clinicians due to its common symptoms and absence of any histopathological hallmarks in light microscopy [14]. Electron microscopic imaging of renal tissue specimen, showing effacement of the foot processes of glomerular podocytes is the only confirmed diagnostic signature for these patients [15]. Progression of MCD often weakens the structural integrity of glomerulus showing overlapping symptoms with other diseases including renal amyloidosis [16]. Besides, few reports have highlighted the misdiagnosis of minimal change disease as renal amyloidosis and vice-versa, hinting a possibility of linkage between them [17, 18].

Considering a lot of its symptoms coinciding with renal amyloidosis, we presumed amyloid formation to be a potential player in minimal change disease. Besides, it is the most prevalent form of glomerular disease subtype evident in Indian cohorts [7, 8, 19, 20]. Thus, it is important to understand its etiology and predisposing pathology, to prevent misdiagnosis in most cases. This can be achieved by tracking the disparities in the cellular pathways underlying MCD phenotype. Cellular pathways are the major outcome of several interactions between the biomolecules. Several multi-omics approach like genomics, transcriptomics, proteomics and metabolomics are utilised to capture these interactions [21]. In the recent years, metabolomics has emerged as the robust tool for identifying the functional relevance of small metabolites, key components of vital cellular pathways [22]. Untargeted metabolomics approach is preferred over targeted, owing to the unbiased identification of both known and unknown metabolites with a broader perspective [23, 24].

In this study, we have shown the putative role of amyloid formation in driving the pathology associated with MCD. Further, using high-throughput mass spectrometry-based untargeted approach we have identified a panel of altered metabolites in renal amyloidosis cases having minimal change disease as compared to controls.

2. Materials and methods

2.1 Sample collection

In a two-year single centre study carried out from 2018 to 2020, 400 patients with renal impairment were examined based on the symptoms and abnormal renal function test (RFT) profile. Out of these, 100 patients were suspected of glomerular disease based on haematuria, hypoalbuminemia and nephrotic range proteinuria. For further evaluation, renal biopsy specimen was obtained from the cortex region of the affected kidney (after taking the informed consent). In addition, 2ml of blood was also collected from these patients and controls (having normal renal function) in an EDTA containing vacutainer and was subjected

to centrifugation (1000 x g for 10 minutes at 4ºC) to collect the plasma. Ethics approval (**Ref No** IITK/IEC/2017-18 II-4 & EC/BMHR/2020/18) for this study was obtained from the human ethics committee of IIT Kanpur and GSVM medical college.

2.3. Histopathological analysis of patient

The renal tissues from each of these suspected patients were obtained via ultrasound-guided renal biopsy. The fresh tissues (collected in saline solution) were then processed followed by paraffin embedding. Finally, a series of staining procedures were performed to identify the pathological hallmarks.

2.3.1 Haematoxylin and Eosin staining of the FFPE tissue sections

5µm thick deparaffinized tissue sections were serially rehydrated in different grades of ethanol (100% to 70%) followed by final rehydration in distilled water. The hydrated sections were then put in Hematoxylin-Mayer's solution (sigma aldrich, catalog number: H9627) for two minutes followed by a brief wash in distilled water and counterstaining with 1% eosin Y (merck millipore, catalog number: 115935) solution for thirty seconds. It was subjected to subsequent dehydration and xylene treatment. Finally, the slides were mounted in mounting media and observed in bright light under a microscope.

2.3.2 Periodic acid Schiff staining of the FFPE tissue sections

The patient derived renal tissue sections were deparaffinised and hydrated to deionised water. It was then immersed in 0.5% periodic acid (Himedia, catalog number: GRM1837) solution for five minutes at room temperature (18-26ºC) followed by rinsing in different changes of distilled water. Next, the sections were then immersed in Schiff's reagent (Merck Millipore, catalog number: 109033) for fifteen minutes at room temperature followed by washing them in lukewarm warm water for five minutes. Finally, it was then counterstained in haematoxylin solution for ninety seconds followed by rinsing in running tap water for 5 minutes. The slides containing stained tissue sections were then dehydrated and mounted in mounting media followed by visualising under the microscope in bright light.

2.3.3 *Congo red staining of the FFPE tissue sections*

The stock and working solutions of Congo red (sigma Aldrich, catalog number: C6277) were prepared according to the published protocols [25]. Deparaffinised tissue sections were stained with haematoxylin solution for two minutes. It was then rinsed with tap water for two minutes and then in distilled water twice for two minutes each. The sections were then placed in Congo red working solution A for twenty minutes. Next, they were transferred to the

Congo red working solution B for twenty minutes. The sections were then rinsed briefly in two changes of absolute ethanol for ten seconds each. Finally, the sections were then cleared of leftover ethanol in two changes of xylene followed by mounting the slide under coverslip in synthetic DPX medium.

2.4 Plasma Metabolomic profiling of patients using a mass spectrometry-based platform

2.4.1 Extraction of metabolites from plasma

400 µl of methanol (Biosolve, catalog number: 136841) was added to 100 µl of plasma, vortexed for 15 seconds and was incubated on ice for 1 hour to allow precipitation of blood proteins. It was then centrifuged in 15,000 x *g* for 15 minutes at 4ºC to remove the precipitated proteins. The supernatant was then lyophilized followed by reconstitution in 50% methanol for further LC-MS analysis.

2.4.2 Separation of extracted metabolites by reverse phase HPLC

The reverse phase chromatography was carried out on an Ultimate 3000UHPLC system (Thermo Scientific). The two mobile phases used for separation consisted of 100% water LC-MS-grade, 10 mM ammonium acetate with 0.1% formic (*v/v*) acid (Sigma Aldrich, catalog number: 09676) (buffer A) and 100% acetonitrile acetonitrile (Biosolve, catalog number: 012041) with 0.1% formic acid (*v/v*) (buffer B). The extracted metabolites were initially re-suspended in 75 µl of 50% methanol and were separated on a C18 Column (ACQUITY UPLC BEH, 130Å, 1.7 µm, 2.1 mm X 100 mm, Waters) with column oven temperature of 30□.The flow rate was set to 200 µl per minute. The linear mobile phase B gradient was applied from 5% to 95%B. The following gradient program was employed: 5% buffer B (100% acetonitrile with 0.1% formic acid) for 1 min, 5% to 40% buffer B in 2 min, 40% buffer B for another 2 min, 40% to 95% buffer B in 10 min, 95% buffer B for 5 min, 5% buffer B in 6 min and 5% buffer B is kept constant for next 5 min. This resulted in a total gradient time of 30 min.

2.4.3 Separation of extracted metabolites by hydrophilic interaction chromatography

The HILIC separation was also performed on the Ultimate 3000 UHPLC system (Thermo Scientific), maintaining column temperature at 30ºC. The mobile phase A was 100% water LC-MS-grade 10 mM ammonium acetate with 0.1% formic (*v/v*) acid and the mobile phase B was 10 mM ammonium acetate solution in 90% LC-MS-grade acetonitrile with 0.1% formic acid (*v/v*). The flow rate was set at 300 µl per minute. A linear gradient of mobile phase B was applied from 95% to 10%. The gradient was as follows: 95% buffer B (90% ACN, LC-

MS-grade with 10 mM ammonium acetate with 0.1%formic) for 0.5 min,90% buffer B in next 1 min, 50% buffer B in next 7 min, 30% buffer B in another 0.5 min, 10% buffer B in 1 minute which is held constant for 2.5 min, buffer B was finally brought to 95% in next 1 min which is kept constant for next 1.5 min. This resulted in a total gradient time of 15 min.

2.4.4 Acquisition of ESI-MS and ESI-MS/MS data

The acquisition was performed on a QTOF mass spectrometer (TTOF 5600+, SCIEX) equipped with an electrospray ionisation source and coupled to an Ultimate 3000 UHPLC system (Thermo Scientific). All samples were scanned over a mass range of 50–1000 *m/z* For both reverse phase and HILIC the analysis was done in both positive and negative mode to ensure complete coverage of metabolome [26]. Mass spectrometer was operated in a data dependent mode. The *m/z* peaks having mass intensity greater than 100 and charge +1 were further subjected to MS/MS fragmentation in each duty cycle. Collision energy was set at 30 eV with a variable window of 15.

2.4.5 Processing of raw MS-spectral data

Peak finding and alignment across the samples was performed using MarkerView v1.2.1 (SCIEX). The peak finding criteria was set as follows: minimum spectral peak width was set to 5 ppm, minimum RT peak width was set to 5 scans, noise threshold of 500 was used and charge state was assigned. For peak alignment, retention time tolerance of 1 min and mass tolerance of 5 ppm was used. Peaks present in less than 70% of samples were filtered out. Only monoisotopic peaks were used for quantification. Data was exported in a spreadsheet format for further analysis.

2.4.6 Statistical analysis

The observed metabolic features were subjected to multivariate statistical analysis using metaboanalyst 5.0 software [27]. Initially the spectral intensities was normalised based on sum of peak area to minimise data variability and make the samples more comparable [28]. Percentage relative standard deviation (RSD%) was calculated on QC samples to assess variability from extraction. Metabolic features, having RSD >40% on the QC samples were excluded before statistical analysis [29]. Further, the normalised data was log transformed and auto scaled. Intrinsic clustering between the samples were evaluated using unsupervised partial component analysis (PCA). Supervised partial least square discriminant analysis (PLS-DA) was done to determine the important metabolic feature that can significantly cluster and differentiate controls from cases [30]. In addition, the validation and predictive

accuracy of the PLS-DA models were estimated using calculated R-square and Q-square values. Besides, univariate analysis like fold change test, t-test and volcano plot was also done to determine the panel of differential metabolites between the two groups [31]. Nevertheless, variable importance in the form of VIP score was calculated based on these PLS-DA models.

2.4.7 Identification of differentially altered metabolites

The panel of metabolic features having VIP score> 1 were identified in Master View software (SCIEX) using SCIEX- all-in-one, HR-MS/MS library with NIST 2017 library bundle. For metabolic feature not identified with the above library, structure matching was performed with the metabolite entries in databases like human metabolome data base (HMDB), METLIN and LIPID MAPS in Peak View v2.2.

3 Results

Presence of blood and excess proteins in urine are the major clinical manifestations encountered in glomerular diseased patients [32]. These symptoms were also observed in our patients suspected for glomerular disease (Table 1). In addition, other symptoms like hepatomegaly, edema and anasarca were also observed in some of these patients. Histopathological examination, using light microscopy showed no visible change in the structure of glomerulus (Figure S1 A, B, Supplementary information). Further, presence of diffuse mesangial hypercellularity in the glomerulus (Figure S1 D, E, Supplementary information) confirmed diagnosis of minimal change disease in 20 out of 100 patients [33]. Interstitial fibrosis characterised by the presence of eosinophilic hyaline like deposits was evident in the interstitial spaces (Figure S1 C, Supplementary information) of these patients. In addition, distended tubules with mild thickening in tubular basement membrane was also seen (Figure S1 F).

3.1 Amyloid deposition in the minimal change diseased patients

Amyloid deposits are well known to appear as amorphous hyaline-like material in the affected tissues [34]. In addition, renal amyloid deposits are accompanied by mesangial hypercellularity in some cases [35, 36]. Thus, the presence of mesangial hypercellularity and hyaline rich material in the renal biopsy sections of these 20 MCD patients made us anticipate that amyloid formation might drive the underlying pathogenesis in these patients. To test this hypothesis, gold standard Congo red (CR) staining was performed on these tissue specimens derived from these MCD patients. Hyaline deposits in the glomerulus (Figure 1A)

and interstitial spaces on 11 out of 20 biopsies exhibited apple green birefringence under polarised light, hinting amyloid presence (Figure 1B, E). Further upon changing the angle of the polariser by 10° either in clockwise or anticlockwise direction, a transformation in the birefringence from apple green to either bluish-green or reddish orange (depending on the orientation of fibrils) was evident on the affected renal tissue specimens (Figure 1C, D, F). Clinicians and pathologists use this property of CR to detect amyloid deposits in the pathogenic tissue specimens and reduce ambiguity.[37, 38]. Thus, it confirmed the amyloid nature of these eosinophilic deposits. Altogether, the observed pathological hallmarks (Table S2, Supplementary information) along with amyloid deposition suggested its putative role as a player in minimal change disease.

Progression of amyloid formation in any disease condition often occurs as the result of metabolic imbalances in the affected patients [39]. Thus, we aimed to track the metabolic perturbations underlying renal amyloidosis in MCD patients. The plasma samples collected from these biopsy-proven amyloid positive 11 MCD patients and 15 controls (Table 1) were utilised for metabolomic analysis accordingly (Figure 2).

3.2 Metabolomic analysis

3.2.1 Analysis of the mass spectrometry data

One of the important attributes of using untargeted metabolomic platform is the ability to replicate each of the LC run for different biological samples. The differential expression is based upon the peak intensity for each m/z (metabolic feature) in untargeted approach. Thus, it is necessary to produce reproducible chromatogram for such analysis. Here, the total ion chromatograms, extracted from PeakView software (SCIEX) for both the HILIC and reverse phase analysis was reproducible for all the samples (Figure S2 Supplementary information). The spectra of one control sample were found to be abrupt and was excluded for further statistical analysis.

3.2.2 Statistical Analysis

Multivariate analysis of the metabolites using unsupervised, principal component analysis (PCA) showed a clear demarcation in the observed features between cases and controls (Figure 3A). A maximum variance of 23.8% was observed in the first principal component and a minimum variance of 6.2% in the fifth component (Figure 3B). In addition, supervised PLS-DA analysis showed differential clustering among the two groups (Figure 4A) with a maximum variance of 18% and a minimum variance of 7.9% (Figure 4B). Predictive accuracy of the model tested with 10-fold cross validation showed good fit of the PLS-DA

model (Figure 5A) with R square and Q-square greater than 0.7 (Figure 5B). Fold change analysis with t-test identified a total of 17 and 122 metabolic features significantly to be up-regulated and down-regulated respectively in patients as compared to controls (Figure 6A). Based on the calculated variable importance projection (VIP) score (using PLS-DA models), 80 metabolic features (m/z values) were noted to be altered.

3.2.3 Differential distribution and expression of identified metabolites among the two groups

A total of 15 biologically important metabolites with false discovery rate (FDR) less than 0.05 and VIP score greater than 1 (Figure 6B) were identified to be significantly altered between the patients and controls. Initially, all these metabolites were subjected to clustering analysis based on the VIP scores. The generated heat map highlighted their differential expression and clustering among cases and controls (Figure 7). Besides, these metabolites showed differential distribution among the two study groups (Figure S3, Supplementary information). A different list of metabolites was discerned in this study unlike reported for other glomerular diseases (Table S2, Supplementary information). An increased concentration of L-cystine and different carnitines was observed in patients in comparison to controls (Table 2). Similarly, several classes of lipids were found to be downregulated in MCD patients having renal amyloidosis (Table 3). The chromatographic representation of mass ion intensities from cases and controls for some of these altered metabolites, identified in this study also reflected the same pattern (Figure S4, Supplementary information). This in turn validated our observations and analysis.

4 Discussion

The present study has depicted amyloid formation as one of the promising predisposing risk factors underlying the pathogenesis of a glomerular disease subtype, minimal change disease. Damage to the glomerular filtration barrier in the affected patients often leads to disruption of the blood and urine proteins [13]. As a result, these proteins tend to accumulate, and this might account for the amyloid formation and deposition at the injured sites of the kidney in MCD patients.

Another important diagnostic tool for understanding disease-associated pathologies is the assessment of biological markers [40]. They are the key indicators of the intricate cascade of molecular events underlying a disease condition. Identification of potential biomarkers in biological fluids promotes better understanding of disease onset and progression [41]. Previous studies have showcased the role of biological markers in early

diagnosis of amyloid-associated disorders [29, 42-46]. Despite of the presence of biological markers signifying renal failure and its associated diseases [47, 48], distinct diagnostic markers for renal amyloidosis has not been explored till date. Thus, in this study we have fingerprinted the metabolic signatures in MCD patients having renal amyloidosis.

Using LC-MS based untargeted metabolomic platform, the current study has identified a broad array 15 plasma metabolites, significantly altered in MCD-associated renal amyloidosis patients. Out of these L-cystine and different carnitines levels were found to be significantly upregulated whereas, different lipid classes were distinctly found to be downregulated in MCD patients having renal amyloidosis unlike reported for MCD patients alone (Table S2, Supplementary information).

Increased levels of acyl carnitines like adipoyl-L-carnitine and 3-methylglutarylcarnitine were found in the MCD patients having amyloidosis. Acyl carnitines serve as the markers for lipid metabolism in mitochondria. Impairment in mitochondrial function causes dysregulation of the fatty acid metabolism, leading to the upregulation of acyl carnitines in blood [49-51]. Pre-fibrillar amyloid proteins are known to induce mitochondrial dysfunction [52]. In addition, renal fibrosis is often accompanied by mitochondrial dysfunction [53, 54]. In the present study, 11 MCD patients showed the presence of both amyloid deposits and interstitial fibrosis in their kidney. Thus, we speculate that the underlying pathology might account for the upregulation of carnitine and acyl carnitines in these patients, suggesting their putative role as future diagnostic markers. However, elevation of lactate in mitochondrial dysfunction is usually condition dependent [55], accounting for the reduced lactate levels in our cases as compared to controls.

Mitochondrial dysfunction predisposes oxidative stress, an imbalance in the formation of reactive oxygen species (ROS) and subsequent antioxidants [56]. The generated ROS causes oxidative modification of cysteine residues to form L-cystine [57], a sensitive marker reported for redox stress [58]. Oxidative stress serves as an independent risk factor for amyloid formation and its associated pathogenesis [59, 60]. Thus, the presence of oxidative stress in these amyloidosis patients underlying MCD might have caused an increase in the plasma L-cystine levels. Fatigue is reported to be associated with lower levels of linoleyl carnitine in plasma [61]. Hence, the down regulation of linoleyl carnitine in this study signifies fatigue condition, a underlying symptom for impairment of mitochondrial function [62].

Renal amyloidosis results in substantial weight loss of the affected patients [63-65]. One of the important indicators for weight loss is decreased levels of lysophosphatidylcholine

in plasma [66]. In the present study, reduced levels of different classes of phosphatidylcholine and lysophosphatidylcholine might attribute to the amyloidosis-associated weight loss in these patients.

Monoacylglycerols are the major breakdown product of triglycerides via lipase enzyme. Chronic renal failure is associated with elevated levels of apoC-III, a known inhibitor for lipase enzyme [67]. Thus, monoacylglycerol can be a potential candidate to assess the severity of renal impairment in these patients.

In our study the metabolites of several known drugs and plant-based dietary supplements were also identified, probably due to the presence of non-fasting samples. However, these metabolites were not considered for further statistical analysis to reduce ambiguity. The two limitations of this study that could have affected our results are- Firstly it is the limited sample size. Being a pilot study, it needs to be conducted on a large sample size to attain significant clarity. Secondly, all the samples from patients and controls were a mixture of fasting and non-fasting samples as no record was available from the sample collection centre. However, a sub-analysis was performed to trace the dependence of observed metabolome status on nutritional status of the study participants. Five of the identified metabolites mainly di and tri glycerides were excluded after data analysis from list of potential candidates for biomarkers in diagnosis of MCD with amyloidosis. This was done to remove the variation from the fasting/no-fasting state of the blood sample [68].

5 Conclusion

Minimal change disease, a glomerular disease subtype is the underlying cause for idiopathic nephrotic syndrome (INS) in adult patients. In the present study we have highlighted amyloid formation as one of the potential players driving the pathogenesis of minimal change disease in Indian cohort. Additionally, we have utilised LC-MS-based metabolomic platform to capture the dysregulated metabolome underlying amyloid associated pathogenesis in MCD patients. To best of our knowledge, this is the first metabolomic analysis for biomarker discovery in renal amyloidosis underlying MCD, a glomerular disease type. The biological relevance of some these altered metabolites and their linkage to cellular pathways underlying amyloid formation in minimal change disease has been well discussed in this study. This study would set a platform for the clinicians to diagnose early onset and progression of amyloid formation in the kidney of MCD patients. Altogether, it has opened new avenues for discovery of new diagnostic markers in future apart from the currently used painful biopsy-based diagnosis. Despite having statistical significance, the metabolites identified in this

study might not be biochemically significant. Therefore, the clinical applications of these metabolites as potential diagnostic marker need more future studies including validation in a large number of renal amyloidosis patients.

Ethics approval statement

The ethics approval for conducting this study was obtained from the human ethics committee of both GSVM medical college and Indian Institute of Technology Kanpur respectively.

Acknowledgements

SG is thankful to MHRD and IIT Kanpur for funding her PhD fellowship. PS acknowledges CSIR for funding his PhD fellowship. The authors sincerely thank Dr. Richa Giri from GSVM Medical College, Kanpur for her scientific inputs during discussions. They also acknowledge the contribution of Dr. Megha Harke Uppin for validating the histopathological findings.

Author Contributions Statement

AKT supervised the study. SG (I) and AKT designed the experiments. SG (I) conducted all the experiments. PS and SC acquired the mass spectrometry data. SG (I) analysed and interpreted the data with critical input from AKT. SSG mentored PS and SG (I) to analyse and interpret the metabolomics data. SG (II) helped to screen the clinical data and acquire biological samples of the study participants. SG (I) and AKT wrote the manuscript. All the authors read, reviewed and approved the final version of the manuscript.

Disclosure statement

No potential conflict of interest was reported by the author(s).

Abbreviations	
MCD	minimal change disease
FSGS	focal segmental glomerulosclerosis
IgA	immunoglobulin A
US	United States
GFB	glomerular filtration barrier
RFT	renal function test

EDTA	ethylene diamine tetra acetate
ml	millilitre
µl	microlitre
ºC	degree celsius
LC	liquid chromatography
MS	mass spectrometry
FFPE	formalin fixed paraffin embedded
mM	milli molar
CR	Congo red
min	minutes
eV	electron volts
HILIC	hydrophilic interaction liquid chromatography
RT	retention time
ACN	acetonitrile
TOF	time of flight
ppm	parts per million
RSD	relative standard deviation
QC	quality control
PCA	principal component analysis
PLS-DA	partial least square discriminant analysis
VIP	variable importance projection
HMDB	human metabolome database
INS	idiopathic nephrotic syndrome
FDR	false discovery rate
PAS	periodic acid Schiff
TFA	trifluoroacetic acid

References

1. Kitching AR, Hutton HL. The Players: Cells Involved in Glomerular Disease. Clin J Am Soc Nephrol. 2016;11(9):1664-1674.

2. Dattani R, McAdoo S. Secondary glomerular disease. Medicine. 2019;47(10):644-648.
3. O'Shaughnessy MM, Hogan SL, Thompson BD, et al. Glomerular disease frequencies by race, sex and region: results from the International Kidney Biopsy Survey. Nephrology Dialysis Transplantation. 2017;33(4):661-669.
4. O'Shaughnessy MM, Hogan SL, Poulton CJ, et al. Temporal and Demographic Trends in Glomerular Disease Epidemiology in the Southeastern United States, 1986-2015. Clin J Am Soc Nephrol. 2017;12(4):614-623.
5. Jamil M, Bhattacharya PK, Raphael V, et al. Spectrum of Glomerular Diseases in Adults: A Study from North Eastern India. The Journal of the Association of Physicians of India. 2018;66(8):36-39.
6. Muthu V, Ramachandran R, Nada R, et al. Clinicopathological spectrum of glomerular diseases in adolescents: A single-center experience over 4 Years. Indian Journal of Nephrology. 2018;28(1):15-20.
7. Reshi AR, Bhat MA, Najar MS, et al. Etiological profile of nephrotic syndrome in Kashmir. Indian Journal of Nephrology. 2008;18(1):9-12.
8. Agarwal SK, Dash SC. Spectrum of renal diseases in Indian adults. The Journal of the Association of Physicians of India. 2000;48(6):594-600.
9. Rathi M, Bhagat RL, Mukhopadhyay P, et al. Changing histologic spectrum of adult nephrotic syndrome over five decades in north India: A single center experience. Indian Journal of Nephrology. 2014;24(2):86-91.
10. Vanikar A, Kanodia K, Patel R, et al. Primary Immunoglobulin A (IgA) nephropathy in Western India. 2005;15(4):227-231.
11. Paparello JJ: Diagnostic Testing in Glomerular Disease. Glomerulonephritis. 2017:1-2.
12. Vivarelli M, Massella L, Ruggiero B, et al. Minimal Change Disease. Clin J Am Soc Nephrol. 2017;12(2):332-345.
13. Hebert LA, Parikh S, Prosek J, et al. Differential diagnosis of glomerular disease: a systematic and inclusive approach. American journal of nephrology. 2013;38(3):253-266.
14. Fogo AB, Lusco MA, Najafian B, et al. AJKD atlas of Renal Pathology: Minimal Change Disease. American Journal of Kidney Diseases. 2015;66(2):376-377.

15. Owji SM, Shahraki HR, Owji SH, et al. Electron microscopy situation in the diagnosis of minimal change disease; a 16-year survey. Journal of Renal Injury Prevention. 2020;11(4): e15642-e15642.
16. Khalighi MA, Dean Wallace W, Palma-Diaz MF: Amyloid nephropathy. Clinical Kidney Journal. 2014;7(2):97-106.
17. Hetzel GR, Uhlig K, Mondry A, et al. AL-amyloidosis of the kidney initially presenting as minimal change glomerulonephritis. American Journal of Kidney Diseases 2000;36(3):630-635.
18. Sayed RH, Gilbertson JA, Hutt DF, et al. Misdiagnosing renal amyloidosis as minimal change disease. Nephrology Dialysis Transplantation. 2014;29(11):2120-2126.
19. Keskar V, Jamale TE, Kulkarni MJ, et al. Minimal-change disease in adolescents and adults: epidemiology and therapeutic response. Clinical Kidney Journal. 2013;6(5):469-472.
20. Aggarwal HK, Yashodara BM, Nand N, et al. Spectrum of renal disorders in a tertiary care hospital in Haryana. The Journal of the Association of Physicians of India. 2007;55:198-202.
21. Hasin Y, Seldin M, Lusis A. Multi-omics approaches to disease. Genome Biology. 2017;18(1):1-5.
22. Yu L, Li K, Zhang X. Next-generation metabolomics in lung cancer diagnosis, treatment and precision medicine: mini review. Oncotarget. 2017;8(70):115774-115786.
23. Vinayavekhin N, Saghatelian A. Untargeted metabolomics. Current protocols in molecular biology. 2010;90(1):30-31.
24. Ribbenstedt A, Ziarrusta H, Benskin JP. Development, characterization and comparisons of targeted and non-targeted metabolomics methods. PLOS ONE. 2018;13(11):e0207082.
25. Westermark P. Subcutaneous adipose tissue biopsy for amyloid protein studies. Methods in molecular biology. 2012;849:363-371.
26. Nordström A, Want E, Northen T, et al. Multiple ionization mass spectrometry strategy used to reveal the complexity of metabolomics. Analytical Chemistry 2008;80(2):421-429.
27. Pang Z, Chong J, Zhou G, et al. MetaboAnalyst 5.0: narrowing the gap between raw spectra and functional insights. Nucleic Acids Research. 2021;49(W1):W388-W396.

28. Misra BB. Data normalization strategies in metabolomics: Current challenges, approaches, and tools. European Journal of Mass Spectrometry. 2020;26(3):165-174.
29. Olsson M, Hellman U, Wixner J, et al. Metabolomics analysis for diagnosis and biomarker discovery of transthyretin amyloidosis. Amyloid. 2021;28(4):234-242.
30. Worley B, Powers R. Multivariate Analysis in Metabolomics. Current Metabolomics. 2013;1(1):92-107.
31. Grace SC, Hudson DA. Processing and visualization of metabolomics data using R. Metabolomics-fundamentals and applications. 2016:63-94.
32. Modugumudi AS, Venkata PB, Bottla SK, et al. A study of primary glomerular diseases in adults; clinical, histopathological and immunofluorescence correlations. Journal of nephropharmacology. 2016;5(2):91-97.
33. Asma H, Narjess BA, wissal Sahtout A, et al. POS-476 MESANGIAL HYPERCELLULARITY AS A VARIANT OF MINIMAL CHANGE DISEASE: A SERIES OF 4 PATIENTS. Kidney International Reports. 2022;7(2):S212.
34. Picken MM. The Pathology of Amyloidosis in Classification: A Review. Acta Haematologica. 2020;143(4):322-334.
35. Said SM, Sethi S, Valeri AM, et al. Renal amyloidosis: origin and clinicopathologic correlations of 474 recent cases. Clin J Am Soc Nephrol. 2013;8(9):1515-1523.
36. Paueksakon P. Amyloid nephropathy: a practical diagnostic approach and review on pathogenesis. IntechOpen. 2016.
37. Howie AJ, Brewer DB, Howell D, et al. Physical basis of colors seen in Congo red-stained amyloid in polarized light. Laboratory Investigation. 2008;88(3):232-242.
38. Howie AJ, Brewer DB. Optical properties of amyloid stained by Congo red: history and mechanisms. Micron. 2009;40(3):285-301.
39. Brunt EM, Tiniakos DG. Metabolic storage diseases: amyloidosis. Clinics in Liver Disease. 2004;8(4):915-930.
40. Srinitha B. Biomarkers and Disease Diagnosis. Primary Health Care: Open Access 2021;11(4):1-2.
41. Sumner DR, Ross R, Purdue E. Are there biological markers for wear or corrosion? A systematic review. Clinical Orthopaedics and Related Research. 2014;472(12):3728-3739.
42. Baldacci F, Mazzucchi S, Della Vecchia A, et al. The path to biomarker-based diagnostic criteria for the spectrum of neurodegenerative diseases. Expert review of molecular diagnostics. 2020;20(4):421-441.

43. Andersen E, Casteigne B, Chapman WD, et al. Diagnostic biomarkers in Alzheimer's disease. Biomarkers in Neuropsychiatry. 2021;5:100041.
44. Fotiou D, Theodorakakou F, Kastritis E. Biomarkers in AL Amyloidosis. International journal of molecular sciences. 2021;22(20):10916.
45. Jiang X, Labaudinière R, Buxbaum JN, et al. A circulating, disease-specific, mechanism-linked biomarker for ATTR polyneuropathy diagnosis and response to therapy prediction. Proceedings of the National Academy of Sciences. 2021;118(9):e2016072118.
46. Treitz C, Gottwald J, Gericke E, et al. Quantitative proteome profiling provides evidence of an activation of the complement cascade in ATTR amyloidosis. Amyloid. 2022;29(2):102-109.
47. Zabetian A, Coca SG. Plasma and urine biomarkers in chronic kidney disease: closer to clinical application. Current Opinion in Nephrology and Hypertension. 2021;30(6):531-537.
48. Zhang WR, Parikh CR. Biomarkers of Acute and Chronic Kidney Disease. Annual Review of Physiology. 2019;81:309-333.
49. Beger RD, Bhattacharyya S, Gill PS, et al. Acylcarnitines as translational biomarkers of mitochondrial dysfunction. Mitochondrial Dysfunct Caused Drugs Environ Toxic. 2018;1:383-393.
50. Sharma S, Black SM. CARNITINE HOMEOSTASIS, MITOCHONDRIAL FUNCTION, AND CARDIOVASCULAR DISEASE. Drug Discovery Today: Disease Mechanisms. 2009;6(1-4):e31-e39.
51. Liew G, Tse B, Ho IV, et al. Acylcarnitine abnormalities implicate mitochondrial dysfunction in patients with neovascular age-related macular degeneration. Investigative Ophthalmology & Visual Science. 2020;61(8):32-32.
52. J Saraiva M, Magalhaes J, Ferreira N, et al. Transthyretin deposition in familial amyloidotic polyneuropathy. Current medicinal chemistry. 2012;19(15):2304-2311.
53. Zhao H, Liu YJ, Liu ZR, et al. Role of mitochondrial dysfunction in renal fibrosis promoted by hypochlorite-modified albumin in a remnant kidney model and protective effects of antioxidant peptide SS-31. European Journal Pharmacology 2017;804:57-67.
54. Li X, Zhang W, Cao Q, et al. Mitochondrial dysfunction in fibrotic diseases. Cell Death Discovery. 2020;6(1):80.

55. Hubens WHG, Vallbona-Garcia A, de Coo IFM, et al. Blood biomarkers for assessment of mitochondrial dysfunction: An expert review. Mitochondrion. 2022;62:187-204.
56. Marrocco I, Altieri F, Peluso I. Measurement and Clinical Significance of Biomarkers of Oxidative Stress in Humans. Oxidative Medicine and Cellular Longevity. 2017;2017:6501046.
57. van der Reest J, Lilla S, Zheng L, Zanivan S, et al. Proteome-wide analysis of cysteine oxidation reveals metabolic sensitivity to redox stress. Nature Communications. 2018;9(1):1-16.
58. Fu X, Cate SA, Dominguez M, et al. Cysteine Disulfides (Cys-ss-X) as Sensitive Plasma Biomarkers of Oxidative Stress. Scientific Reports. 2019;9(1):1-9.
59. Nakamura M, Ando Y. Amyloidosis and oxidative stress. Rinsho Byori. The Japanese Journal of Clinical Pathology. 2003;51(2):140-145.
60. Bhatti JS, Bhatti GK, Reddy PH. Mitochondrial dysfunction and oxidative stress in metabolic disorders - A step towards mitochondria based therapeutic strategies. Biochimica et Biophysica Acta (BBA) Molecular Basis of Disease. 2017;1863(5):1066-1077.
61. Reuter SE, Evans AM. Long-chain acylcarnitine deficiency in patients with chronic fatigue syndrome. Potential involvement of altered carnitine palmitoyltransferase-I activity. Journal of Internal Medicine. 2011;270(1):76-84.
62. Chazotte B. Mitochondrial Dysfunction in Chronic Fatigue Syndrome. InMitochondria in pathogenesis. 2002:393-410.
63. Sattianayagam PT, Lane T, Fox Z, et al. A prospective study of nutritional status in immunoglobulin light chain amyloidosis. Haematologica. 2013;98(1):136-140.
64. Vaxman I, Gertz M. When to suspect a diagnosis of amyloidosis. Acta Haematologica. 2020;143(4):304-311.
65. Huang X, Wang Q, Jiang S, et al. The clinical features and outcomes of systemic AL amyloidosis: a cohort of 231 Chinese patients. Clinical Kidney Journal. 2014;8(1):120-126.
66. Taylor LA, Arends J, Hodina AK, et al. Plasma lyso-phosphatidylcholine concentration is decreased in cancer patients with weight loss and activated inflammatory status. Lipids in health and disease. 2007;6(1):1-8.

67. Hirano T, Sakaue T, Misaki A, et al. Very low-density lipoprotein-apoprotein CI is increased in diabetic nephropathy: comparison with apoprotein CIII. Kidney international. 2003;63(6):2171-2177.

68. Agueusop I, Musholt PB, Klaus B, et al. Short-term variability of the human serum metabolome depending on nutritional and metabolic health status. Scientific Reports. 2020;10(1):1-3.

List of Tables

Table 1 Characteristics of the glomerular diseased patients suspected of amyloid presence in the kidney

Characteristics	**Mean values ± SD**		**Reference values**
	Cases	***Controls***	
Age (years)	34 ± 11.05	43±14.50	
24-hour urine protein (gm/24hr)	4 ± 2.23	ND	<1gm/24 hr
Serum creatinine (mg/dl)	1.6 ± 0.81	0.84±0.20	0.5-1.5
Serum albumin (gm/dl)	2.5 ± 0.94	4.22±0.39	3.5-5.2
Serum urea (mg/dl)	74 ± 39.76	ND	10-45
Ionic calcium (mg/dl)	4.58 ± 0.44	ND	4.5-5.5

Note: ND- not determined, gm- gram, hr- hour, mg- milligram, dl- decilitre

Table 2 List of biologically important metabolites upregulated in the renal amyloidosis patients with MCD as compared to controls

Metabolite	Observed m/z	Fold Change	p-value	VIP Scores	FDR
Adipoyl-L-carnitine	290.149	9.8369	0.001847	1.7611	2.81E-04
3-Methylglutarylcarnitine	290.149	9.8369	0.001847	1.783	2.81E-04
L-Cystine	239.0141	2.1615	0.005676	1.575	8.38E-04
L-Carnitine	162.1116	2.3463	0.01324	1.25898	0.013124

Note: VIP-variable importance projection score; FDR- False discovery rate

Table 3 List of biologically important metabolites downregulated in the renal amyloidosis patients with MCD as compared to controls

Metabolite	Observed m/z	Fold Change	p-value	VIP Scores	FDR
Lactic acid	89.0241	0.37065	3.58E-09	2.3532	9.91E-11
PC(P-20:0/0:0)	536.4099	0.13097	6.09E-06	2.1304	7.21E-07
MG(i-15:0/0:0/0:0)	317.2693	0.1609	2.46E-05	2.0023	3.01E-06
Chenodeoxycholylglycine	467.3509	0.21824	4.67E-05	2.01172	5.85E-06
1-Myristoyl-sn-glycero-3-phosphocholine	468.3076	0.27637	0.005357	1.6019	8.18E-04
Linoleyl carnitine	424.3245	0.46093	0.028983	1.40784	0.004235
1-Hexadecanoyl-2 octadecadienoyl-sn-glycero-3 phosphocholine	758.5667	0.43265	0.01968	1.4295	0.003068
1-Hexadecyl-sn-glycero-3-phosphocholine	482.3246	0.46309	0.015205	1.50536	0.002349

1-Pentadecanoyl-sn-glycero-3-phosphocholine	482.3246	0.46309	0.015205	1.4607	0.002349
1-Oleoyl-2-myristoyl-sn-glycero-3-phosphocholine	732.5529	0.40485	0.027869	1.41414	0.004162
PC (18:0/0:0)	568.3622	0.38882	0.021899	1.4119	0.003279

Note: VIP-variable importance projection score; FDR- False discovery rate

List of Figures

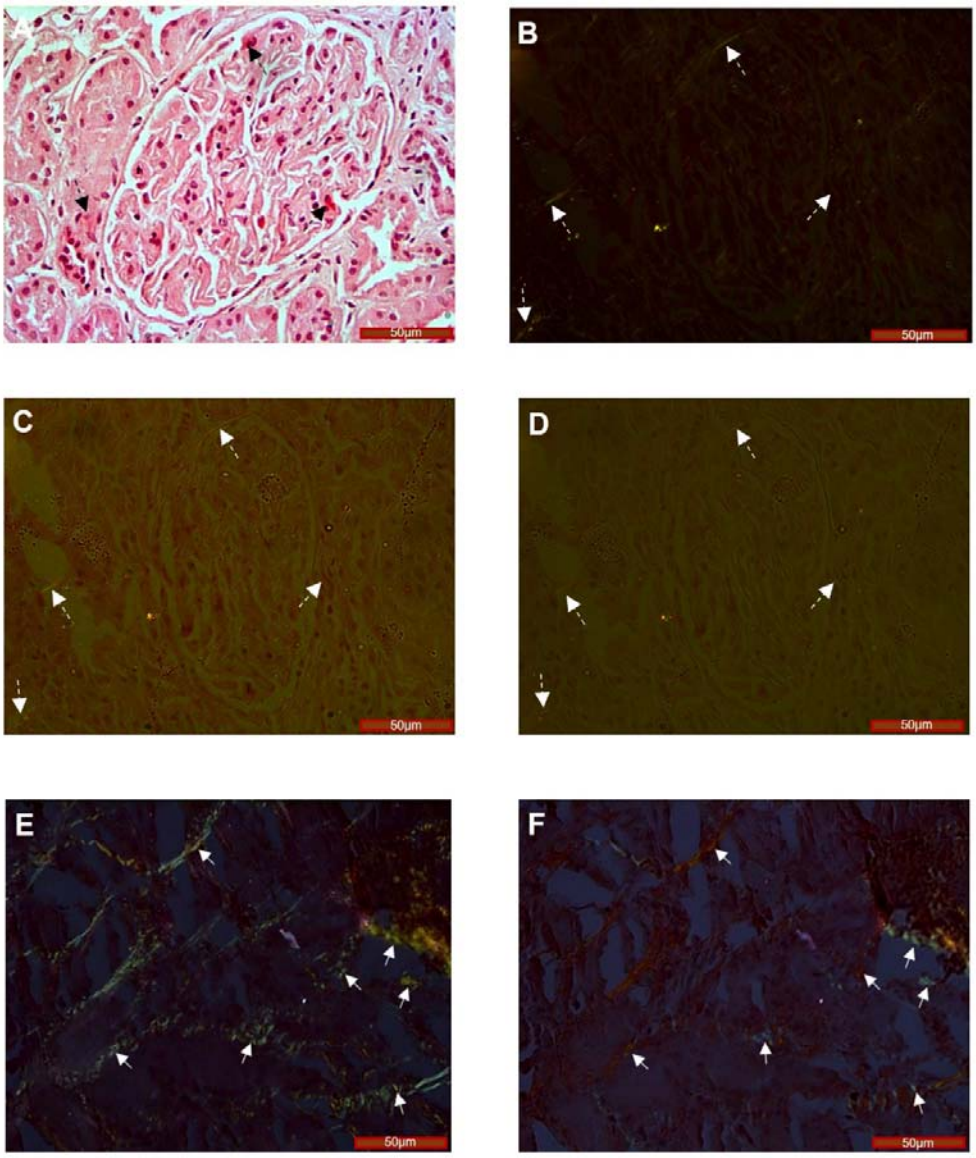

Figure 1 Representative microscopic images of the Congo red stained renal tissue specimen from a glomerular diseased patient suspected of renal amyloidosis. Hyaline rich deposits in the glomerulus (A) (indicated by black dashed arrows) exhibited an apple green birefringence (B) (indicated by white dashed arrows) under polarised light. This was further confirmed by the transformation in birefringence colour from apple green to bluish green or reddish orange upon rotating the polariser by 10º either in clockwise or anticlockwise direction respectively (C, D) (indicated by white dashed arrows). Additionally, amyloid deposits were also observed in the interstitial spaces (E, F) (indicated by white solid arrows). **Scale bar** 50 µm.

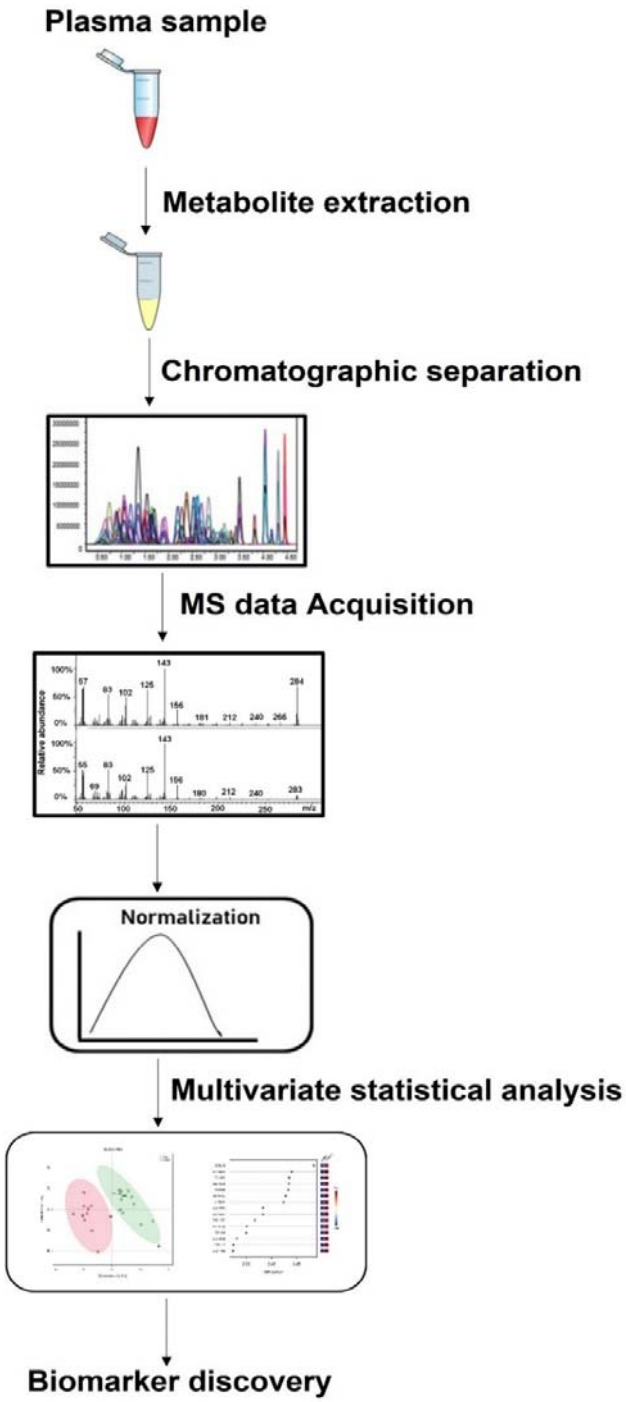

Figure 2 Schematic representation of the workflow for metabolomic analysis.

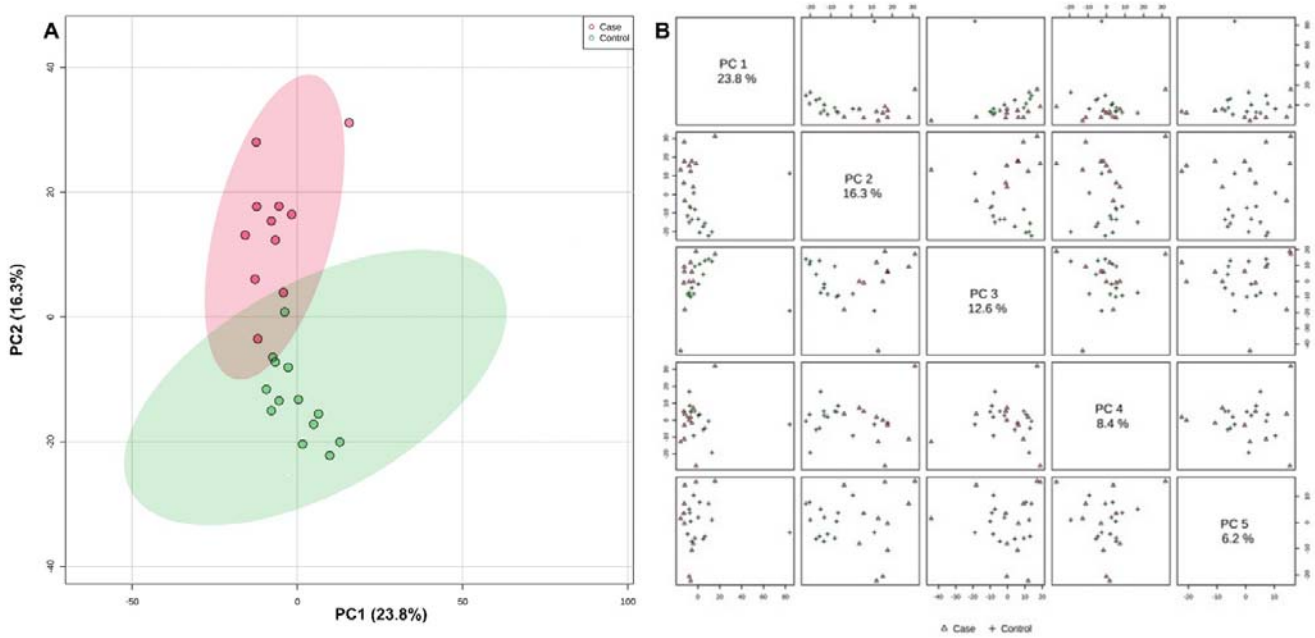

Figure 3 Unsupervised PCA plot depicting differential distribution of metabolic features among two groups (A). A decreasing trend in variance values was observed in all the components of the principal component analysis (B).

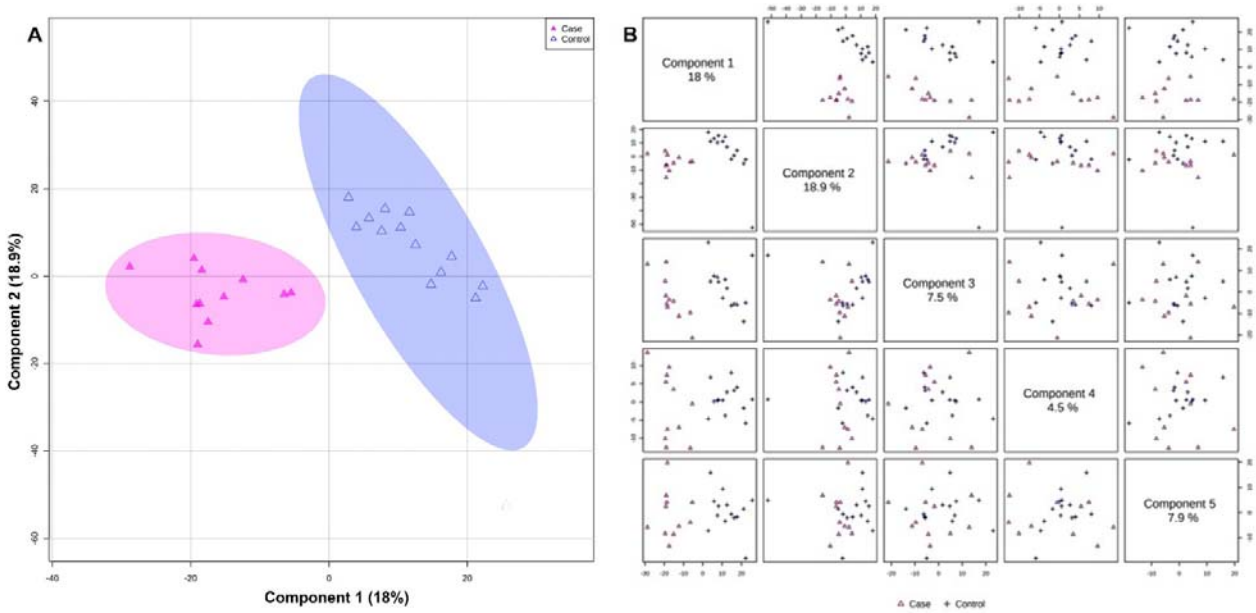

Figure 4 Supervised partial least square discriminant analysis (PLS-DA) model discriminating the metabolic features into two groups (A). A similar decreasing trend in the variance was noted in all the components of the model (B).

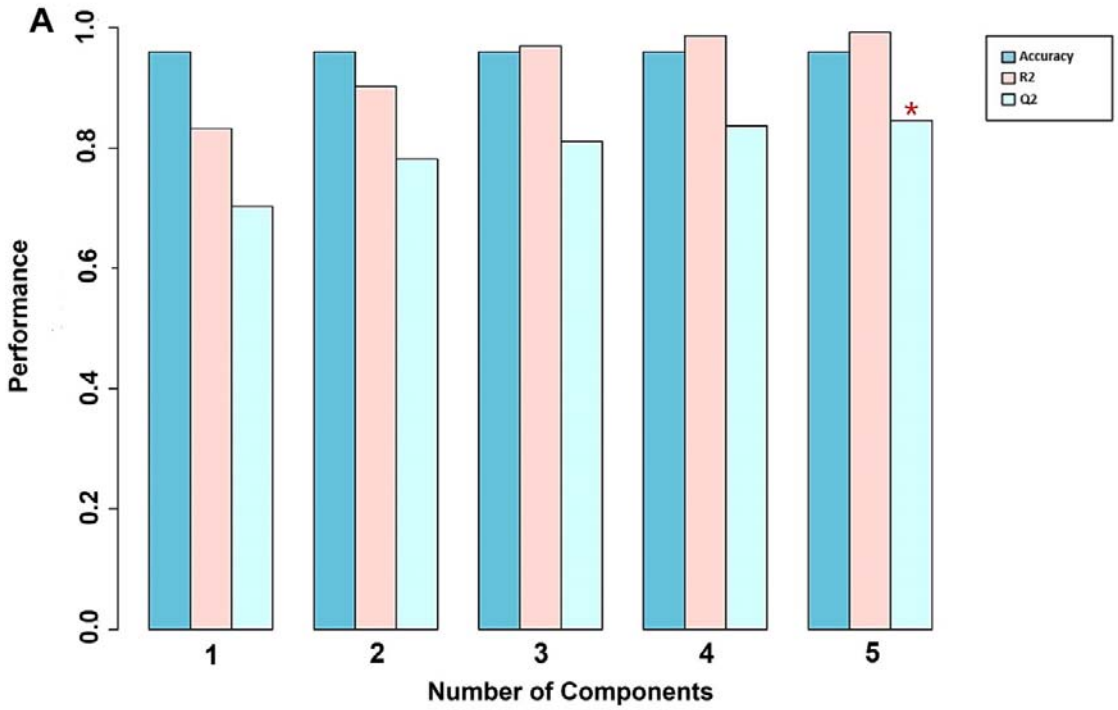

B

Measure	1 comps	2 comps	3 comps	4 comps	5 comps
Accuracy	0.96	0.96	0.96	0.96	0.96
R2	0.83186	0.90168	0.96897	0.98618	0.99197
Q2	0.70261	0.78167	0.81036	0.8371	0.84589

Figure 5 Predictive ability of the PLS-DA model based on 10-fold cross validated Q2 values (A) showing accuracy, R-square and Q-square values of greater than 0.7 (B). This indicated the reliability of the model in predicting the metabolic changes among the two groups. The red star in A represents the best classifier model.

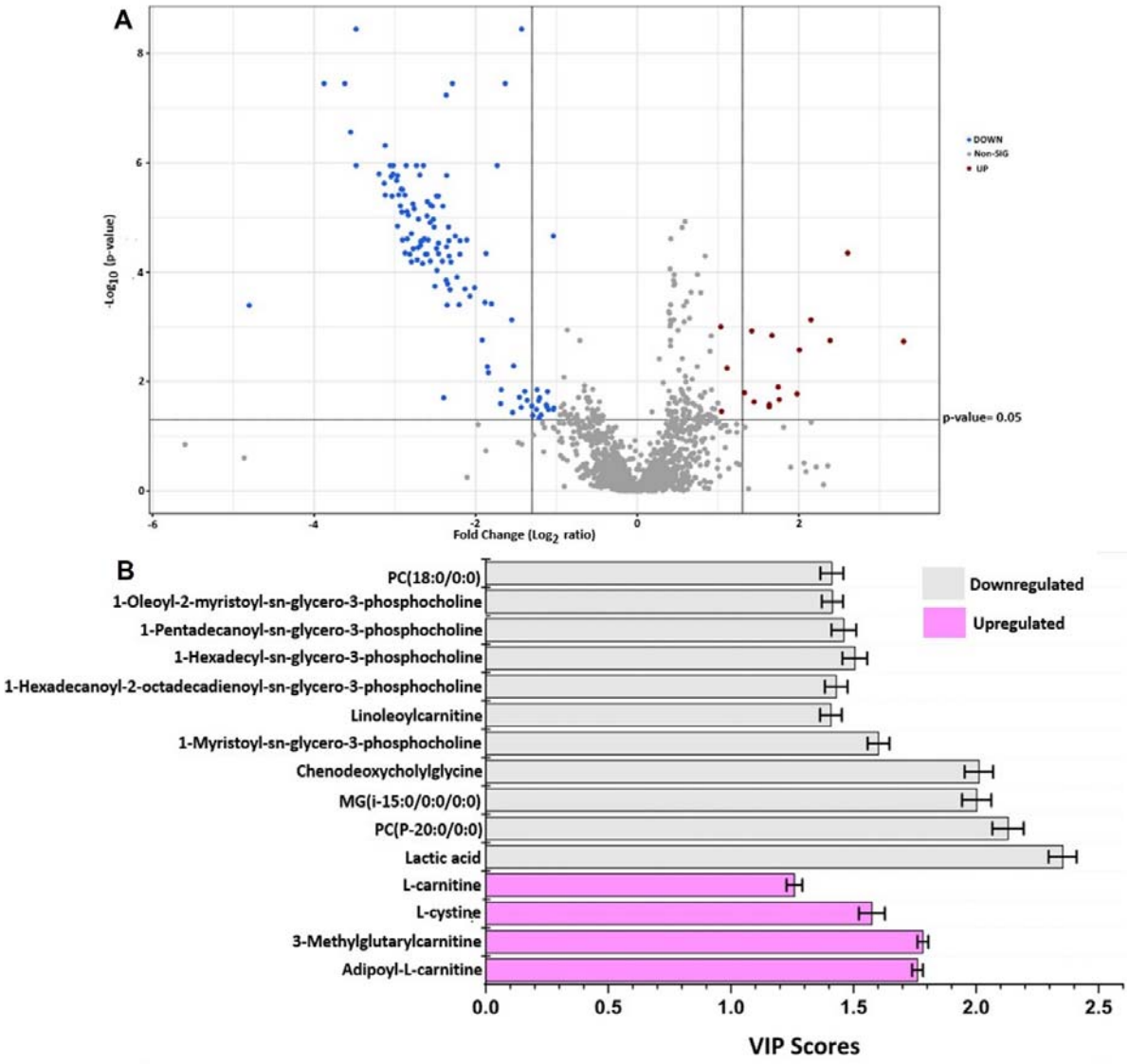

Figure 6 Volcano plot analysis depicted differentially expressed metabolic features (A) in patients as compared to controls (A). The variable importance projection score plot highlighted important 15 metabolites with VIP score greater than 1, discriminating patients from controls (B).

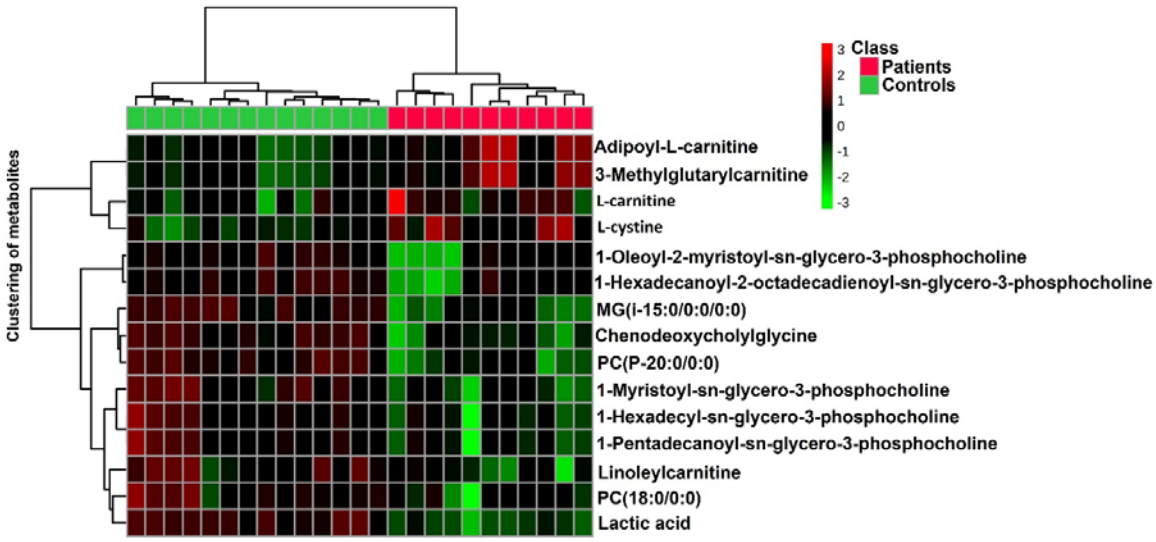

Figure 7 Heat-map analysis showed differential expression of these 15 important metabolites between patients and controls. Each coloured cell on the map represents concentration values of the identified metabolites in different samples.

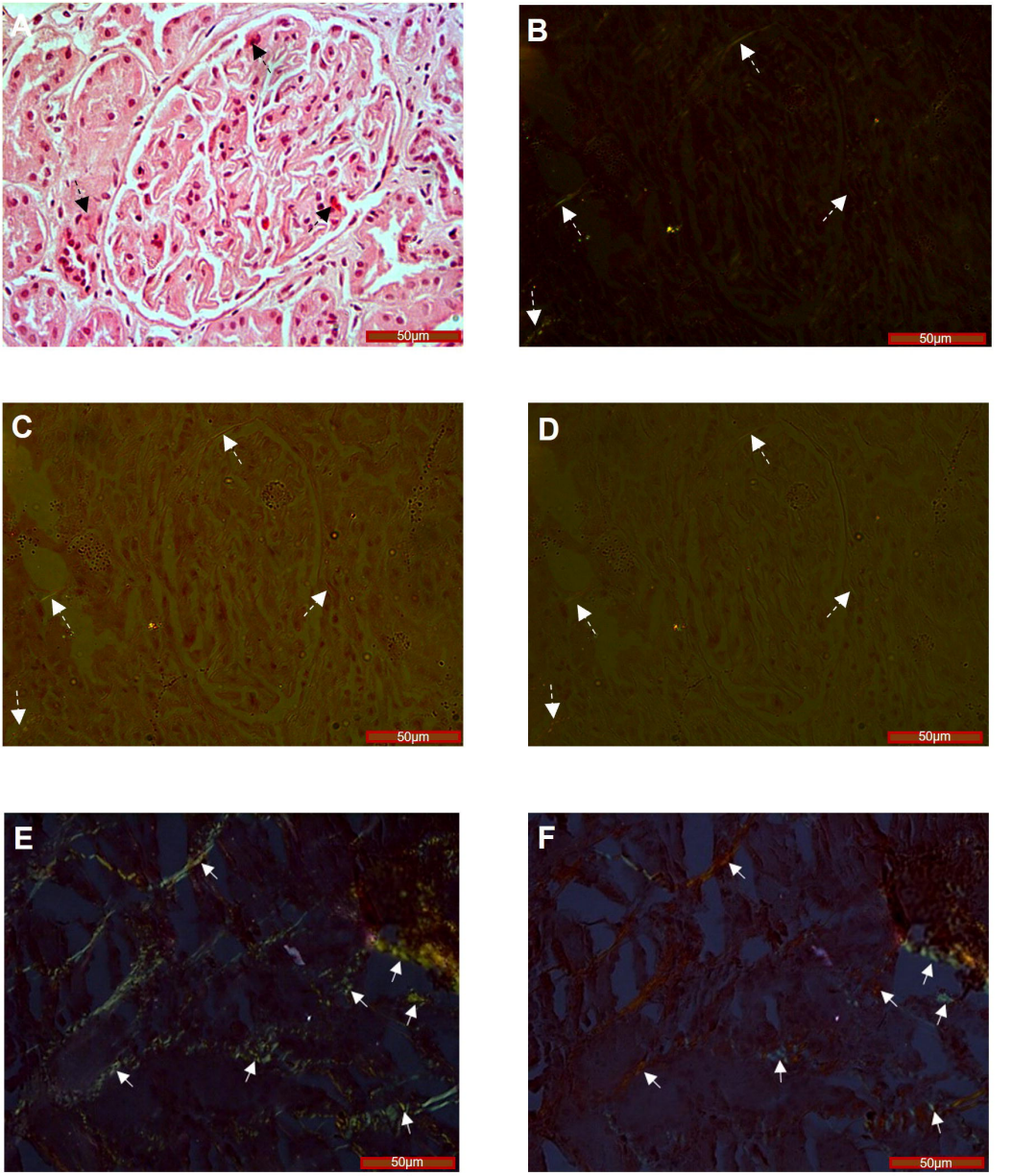
A
50μm
B
50μm
C
50μm
D
50μm
E
50μm
F
50μm

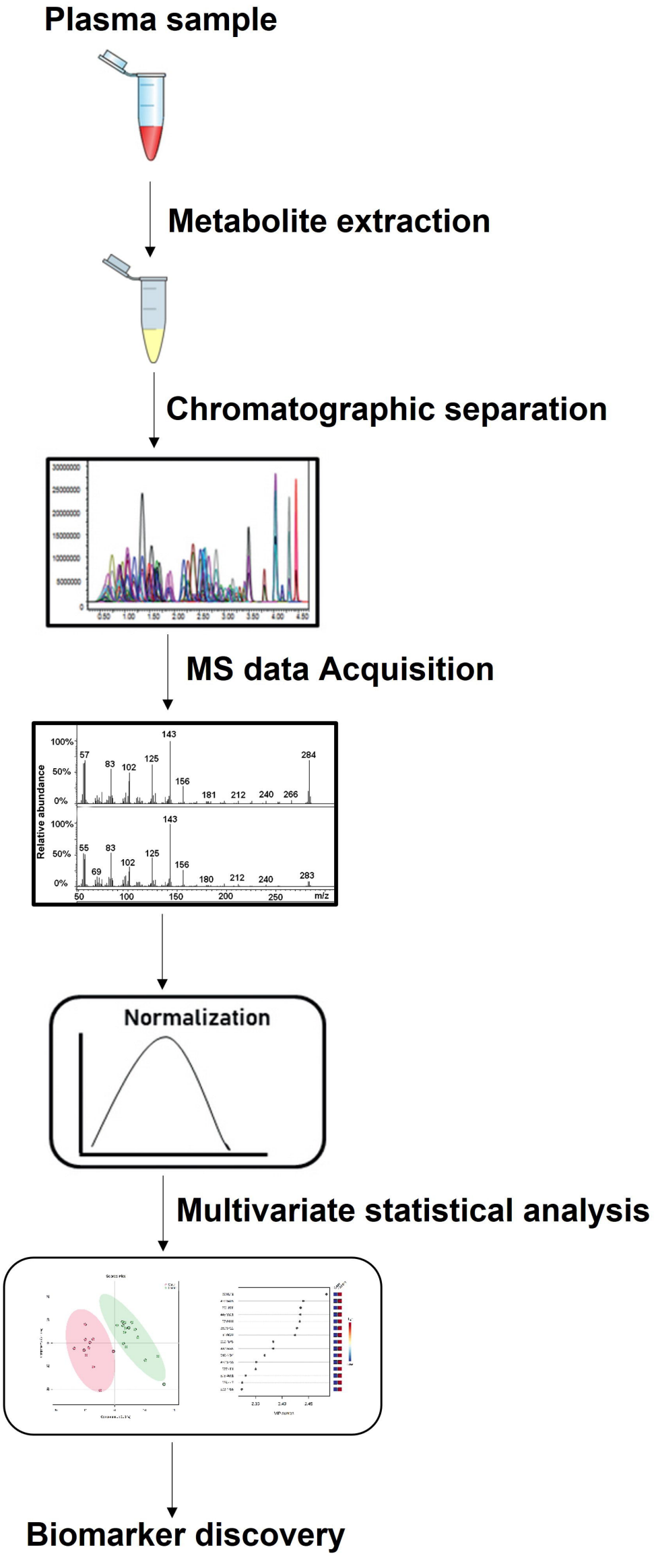
Plasma sample
Metabolite extraction
Chromatographic separation
MS data Acquisition
Relative abundance
m/z
Normalization
Multivariate statistical analysis
Biomarker discovery

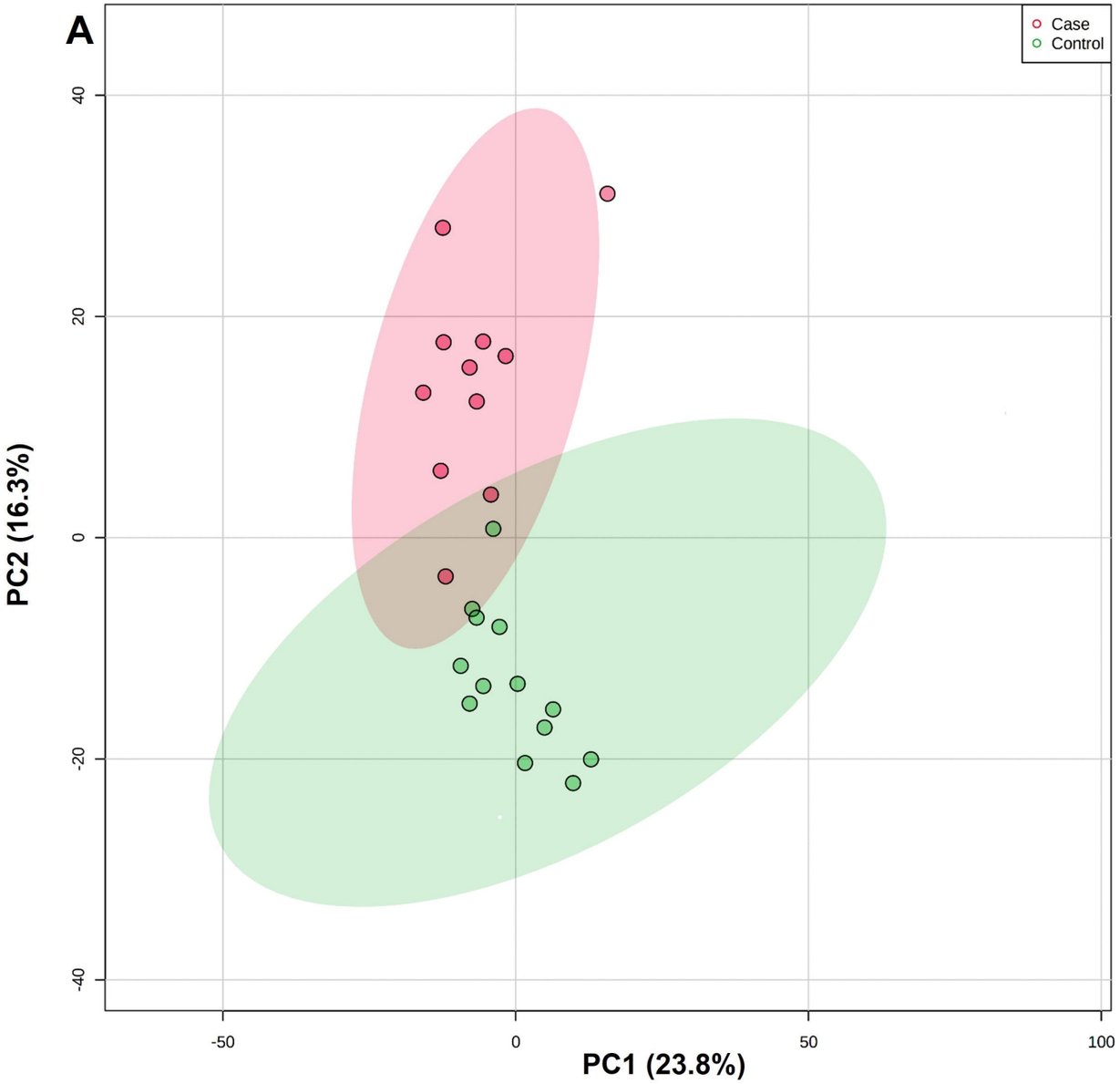
A
Case
Control
PC2 (16.3%)
PC1 (23.8%)
40
20
0
-20
-40
-50
0
50
100

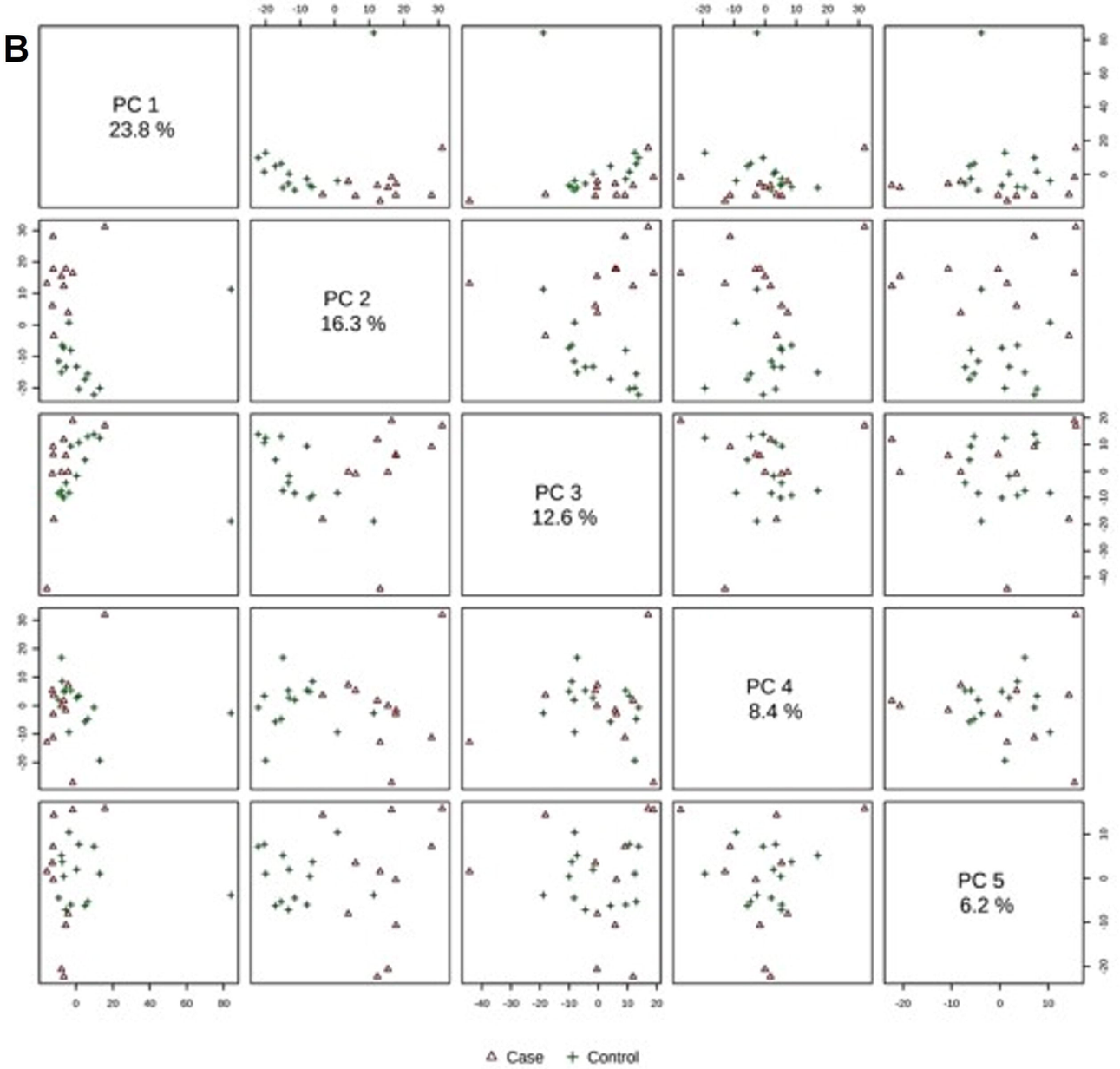
B
PC 1
23.8 %
PC 2
16.3 %
PC 3
12.6 %
PC 4
8.4 %
PC 5
6.2 %
Case
Control

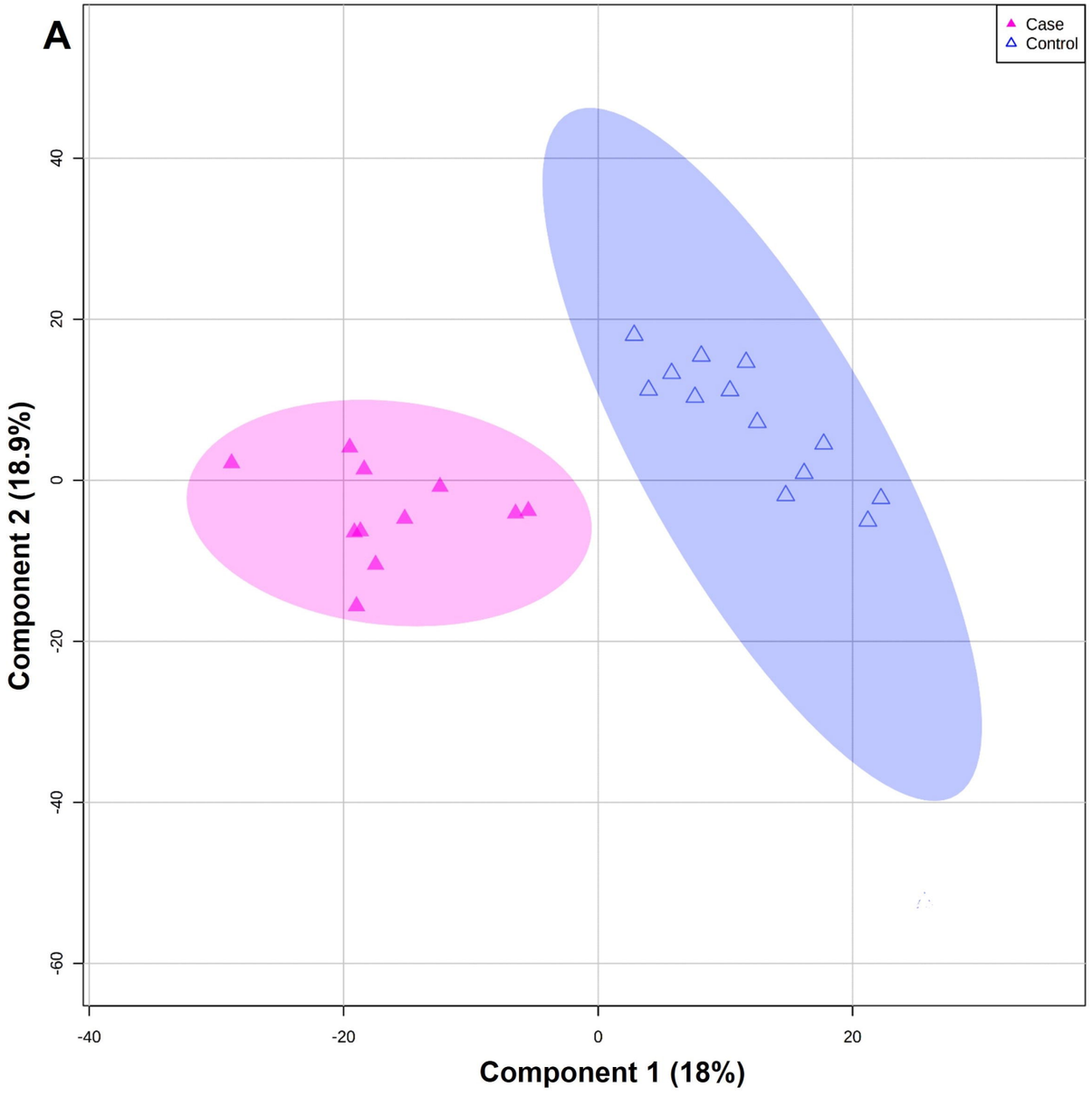
A
Case
Control
Component 2 (18.9%)
Component 1 (18%)
40
20
0
-20
-40
-60
-40
-20
0
20

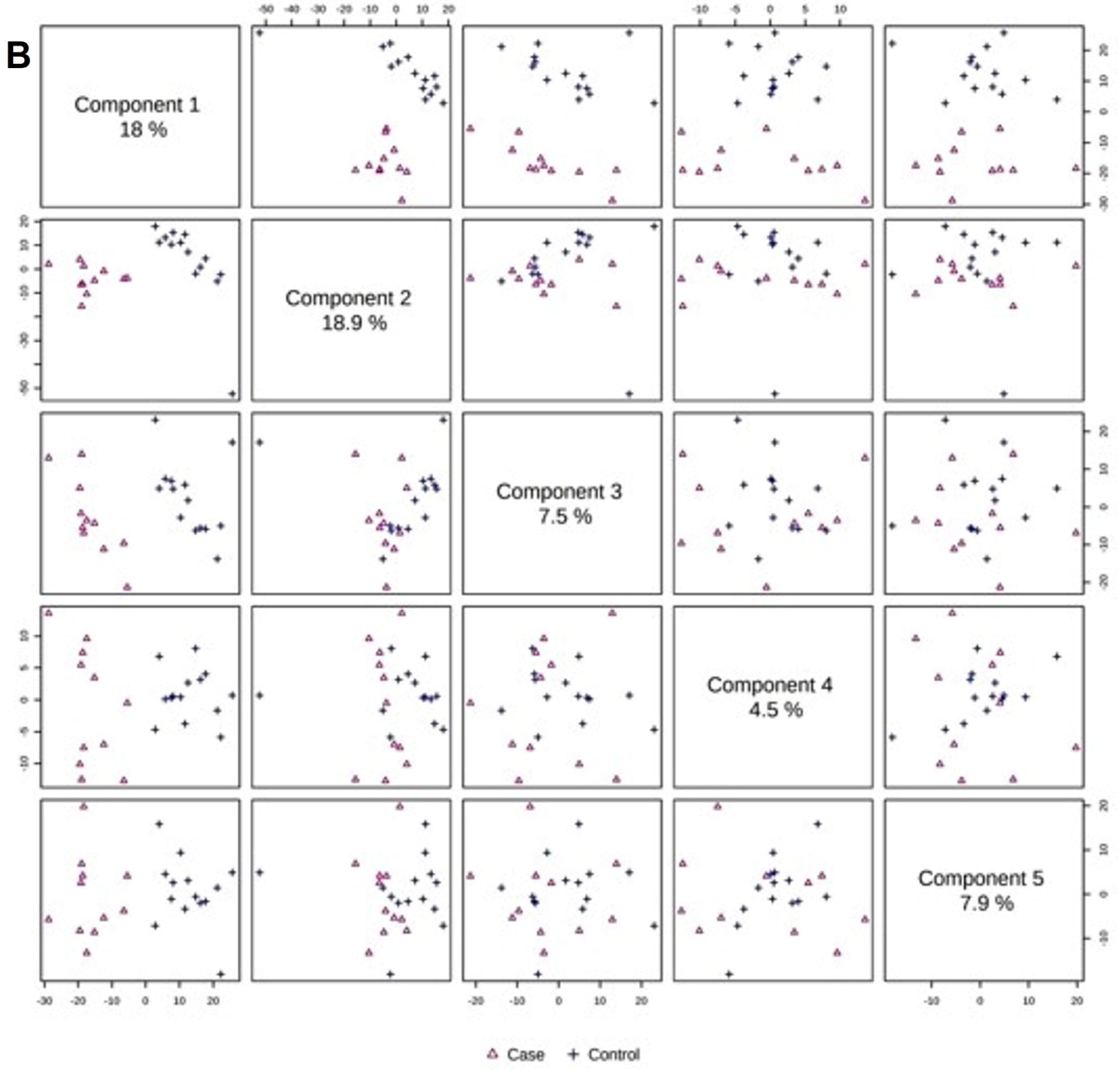
B
Component 1
18 %
Component 2
18.9 %
Component 3
7.5 %
Component 4
4.5 %
Component 5
7.9 %
Case
Control

A

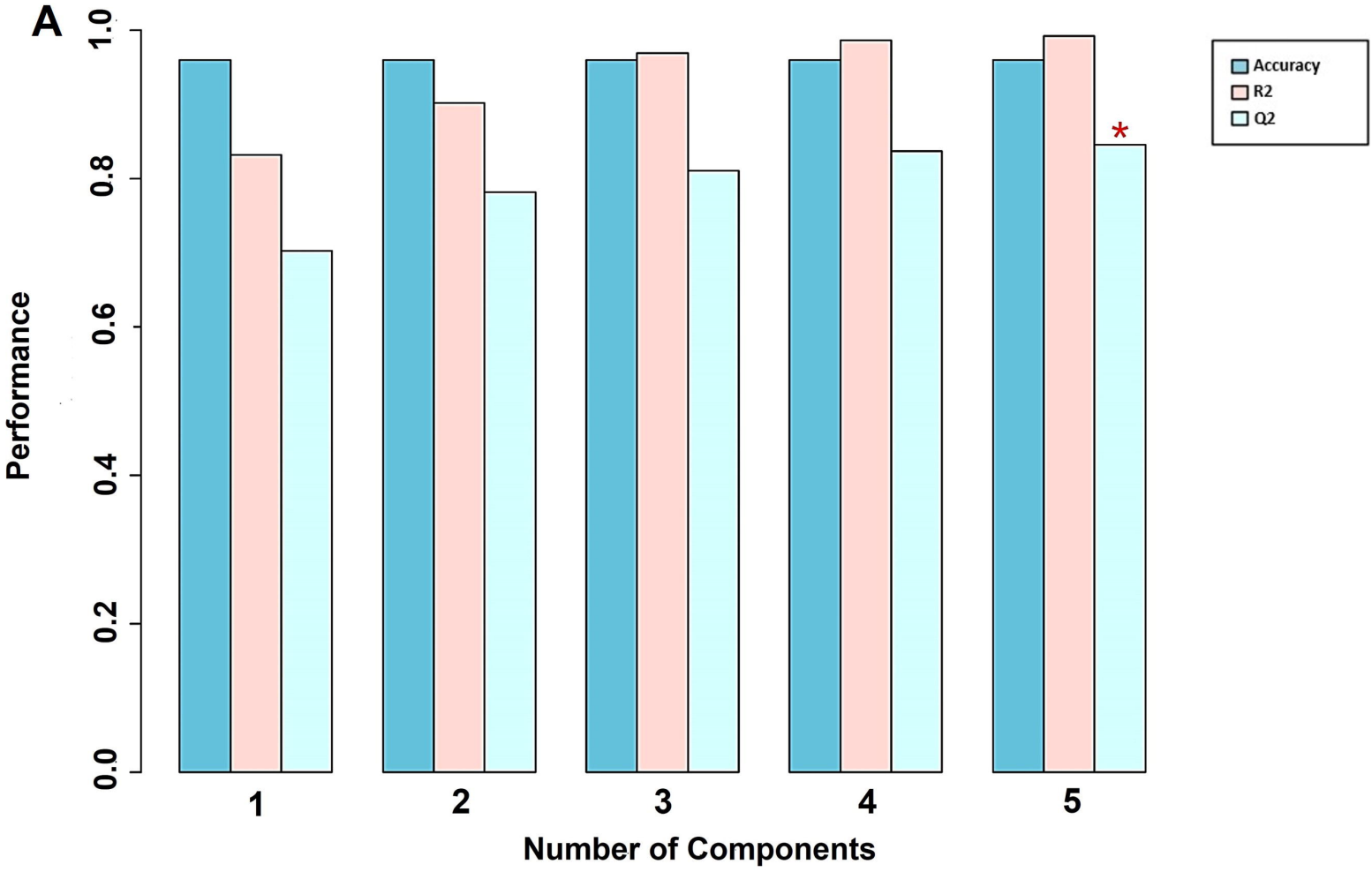

B

Measure	1 comps	2 comps	3 comps	4 comps	5 comps
Accuracy	0.96	0.96	0.96	0.96	0.96
R2	0.83186	0.90168	0.96897	0.98618	0.99197
Q2	0.70261	0.78167	0.81036	0.8371	0.84589

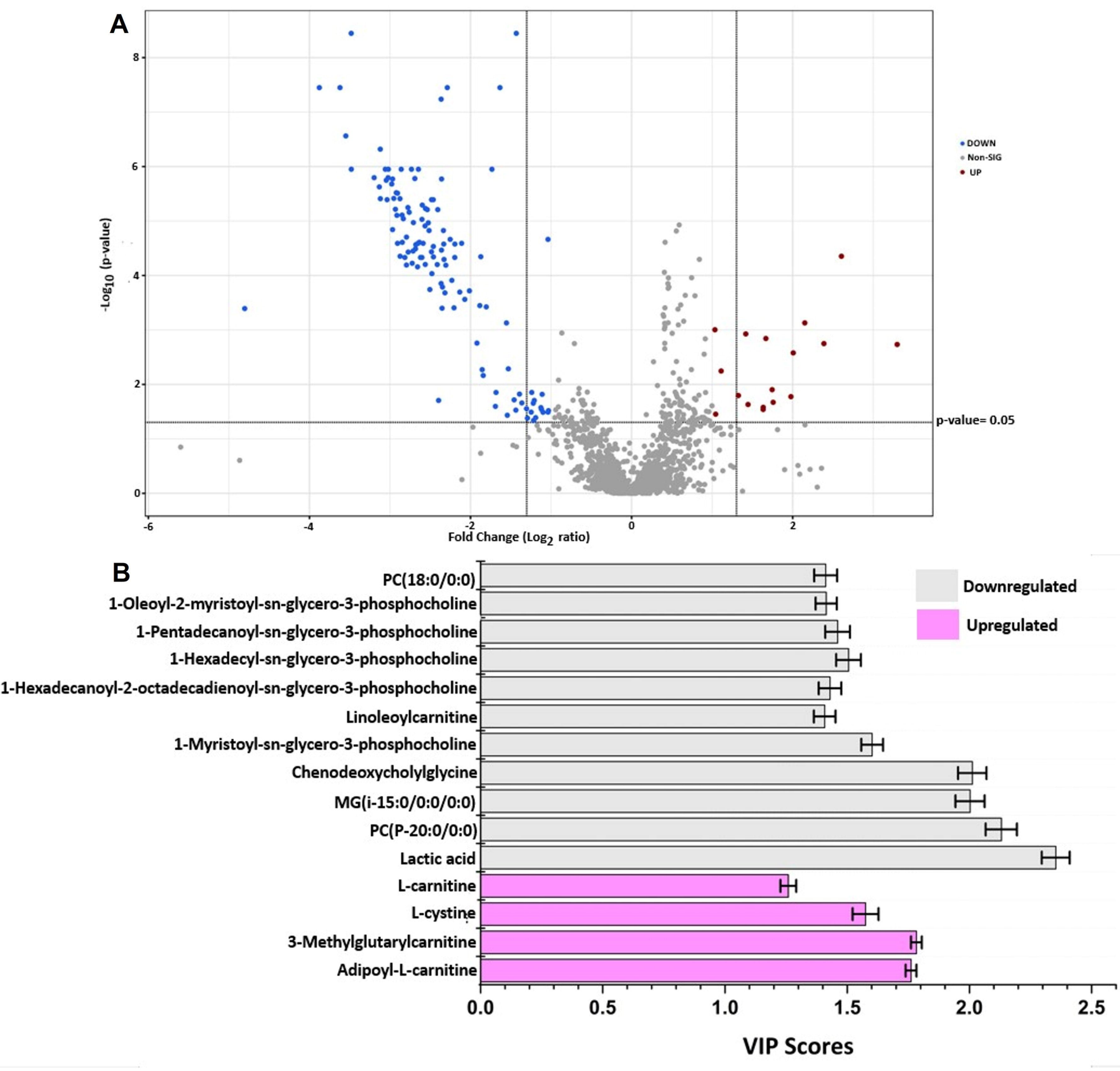
A
DOWN
Non-SIG
UP
p-value= 0.05
-Log10 (p-value)
Fold Change (Log2 ratio)
B
Downregulated
Upregulated
PC(18:0/0:0)
1-Oleoyl-2-myristoyl-sn-glycero-3-phosphocholine
1-Pentadecanoyl-sn-glycero-3-phosphocholine
1-Hexadecyl-sn-glycero-3-phosphocholine
1-Hexadecanoyl-2-octadecadienoyl-sn-glycero-3-phosphocholine
Linoleoylcarnitine
1-Myristoyl-sn-glycero-3-phosphocholine
Chenodeoxycholylglycine
MG(i-15:0/0:0/0:0)
PC(P-20:0/0:0)
Lactic acid
L-carnitine
L-cystine
3-Methylglutarylcarnitine
Adipoyl-L-carnitine
VIP Scores

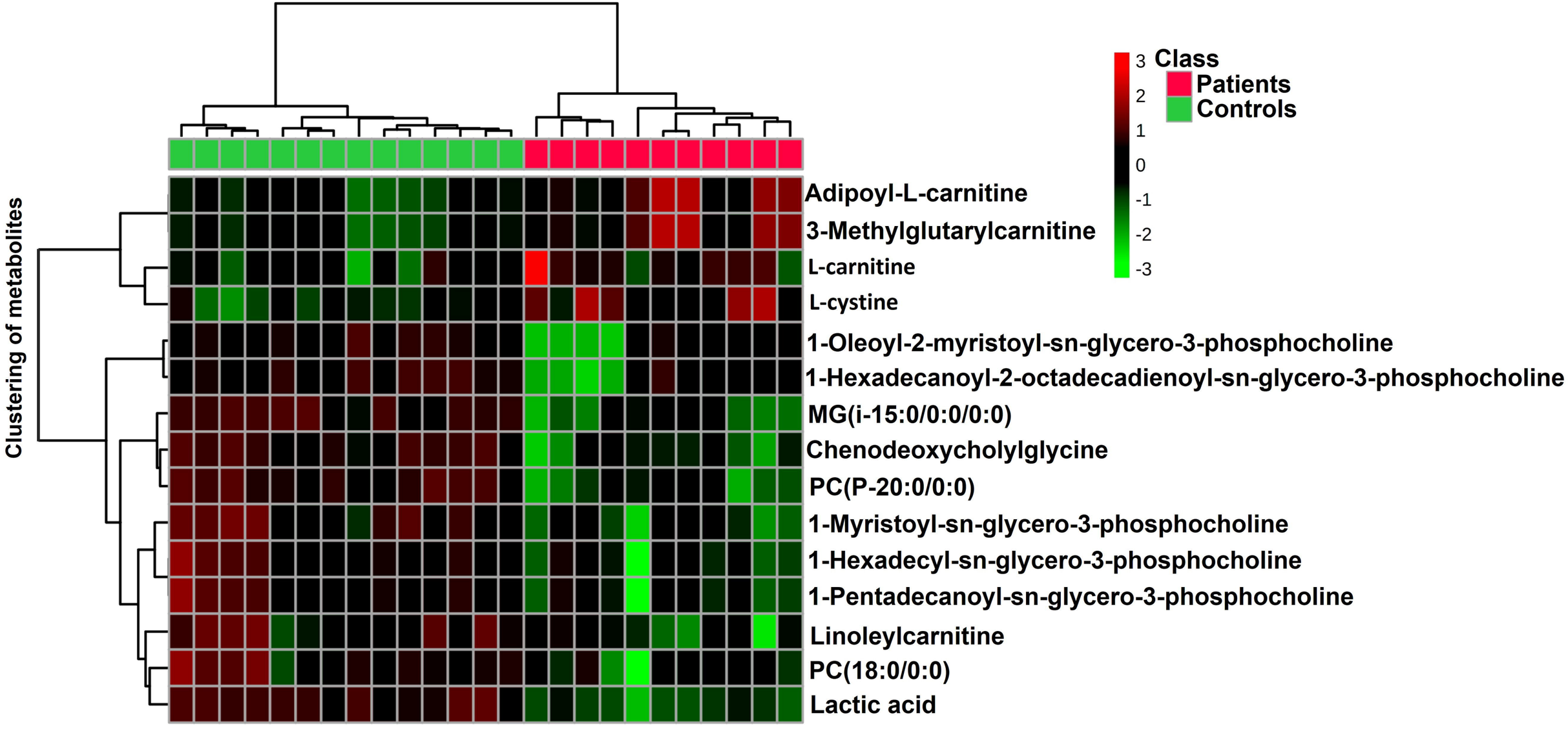
Class
Patients
Controls
3
2
1
0
-1
-2
-3
Clustering of metabolites
Adipoyl-L-carnitine
3-Methylglutarylcarnitine
L-carnitine
L-cystine
1-Oleoyl-2-myristoyl-sn-glycero-3-phosphocholine
1-Hexadecanoyl-2-octadecadienoyl-sn-glycero-3-phosphocholine
MG(i-15:0/0:0/0:0)
Chenodeoxycholylglycine
PC(P-20:0/0:0)
1-Myristoyl-sn-glycero-3-phosphocholine
1-Hexadecyl-sn-glycero-3-phosphocholine
1-Pentadecanoyl-sn-glycero-3-phosphocholine
Linoleylcarnitine
PC(18:0/0:0)
Lactic acid

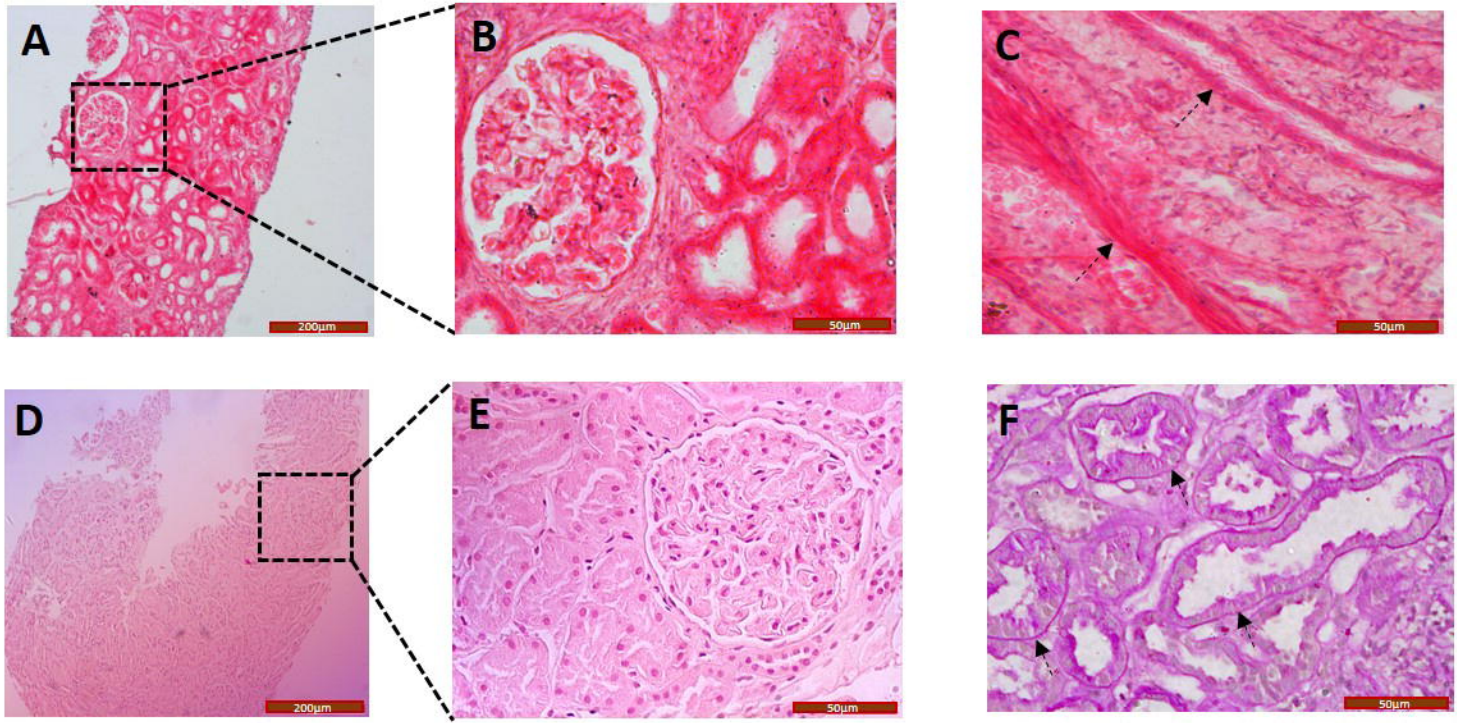
A
200µm
B
50µm
C
50µm
D
200µm
E
50µm
F
50µm

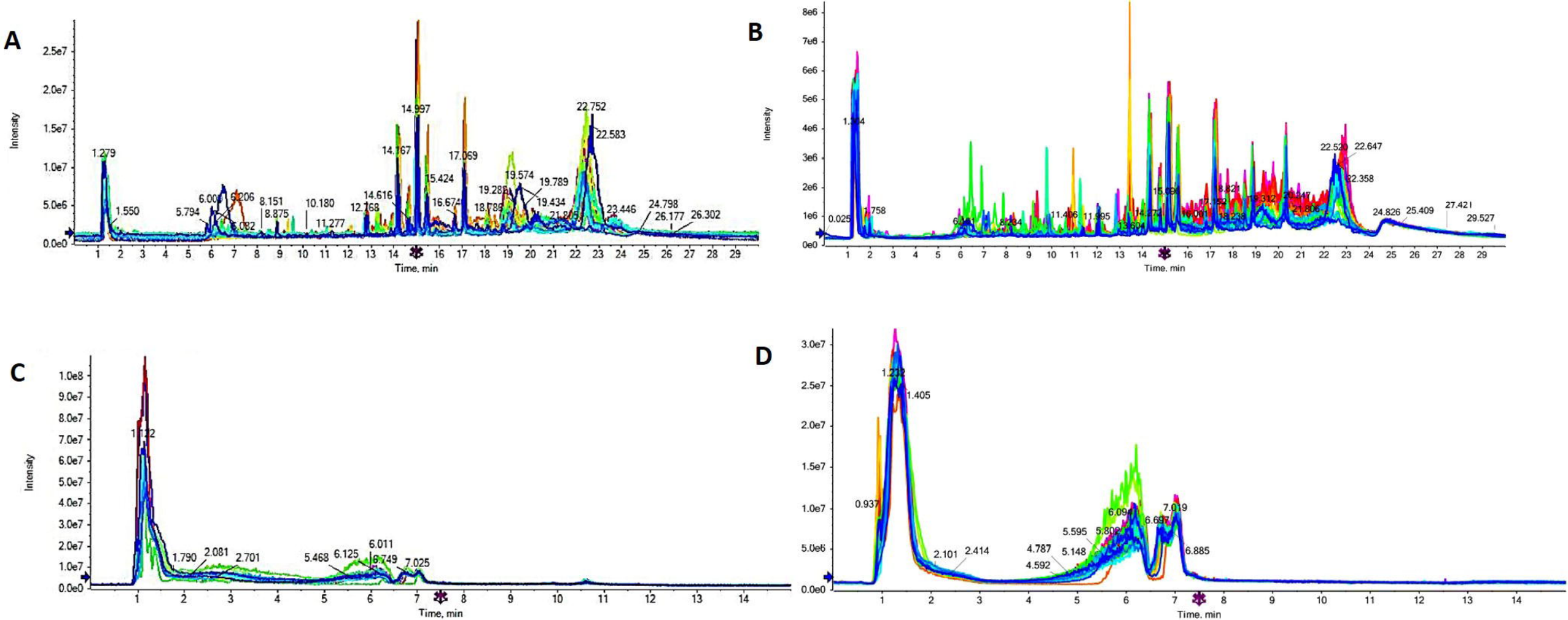
A
B
C
D
Intensity
Time, min
1.279
1.550
5.794
6.008
6.206
6.082
8.151
8.875
10.180
11.277
12.768
14.616
14.167
14.997
15.424
16.674
17.069
18.789
19.288
19.574
19.789
19.434
21.805
22.752
22.583
23.446
24.798
26.177
26.302
0.025
1.758
11.406
11.995
22.520
22.647
22.358
24.826
25.409
27.421
29.527
1.790
2.081
2.701
5.468
6.125
6.011
6.749
7.025
0.937
1.232
1.405
2.101
2.414
4.787
4.592
5.148
5.595
5.802
6.094
6.697
7.019
6.885

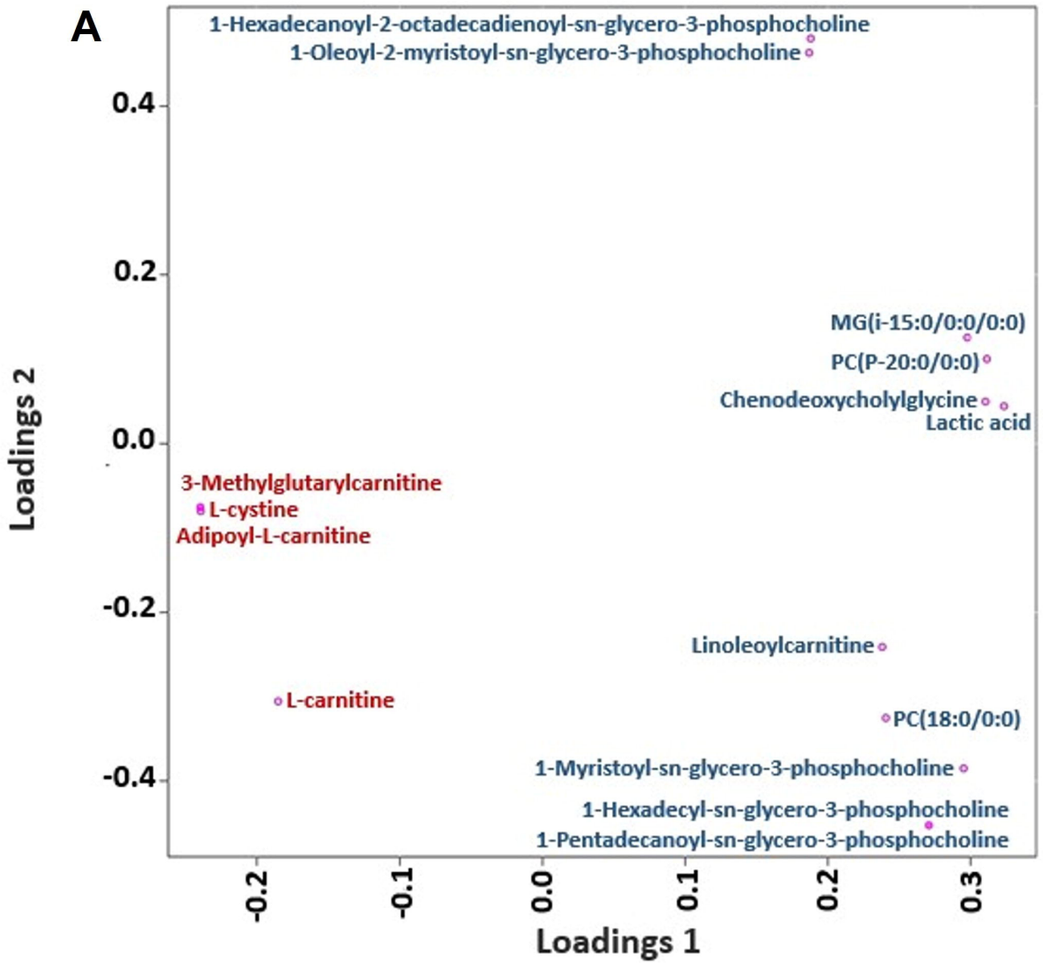
A
1-Hexadecanoyl-2-octadecadienoyl-sn-glycero-3-phosphocholine
1-Oleoyl-2-myristoyl-sn-glycero-3-phosphocholine
MG(i-15:0/0:0/0:0)
PC(P-20:0/0:0)
Chenodeoxycholylglycine
Lactic acid
3-Methylglutarylcarnitine
L-cystine
Adipoyl-L-carnitine
Linoleoylcarnitine
L-carnitine
PC(18:0/0:0)
1-Myristoyl-sn-glycero-3-phosphocholine
1-Hexadecyl-sn-glycero-3-phosphocholine
1-Pentadecanoyl-sn-glycero-3-phosphocholine
Loadings 2
0.4
0.2
0.0
-0.2
-0.4
-0.2
-0.1
0.0
0.1
0.2
0.3
Loadings 1

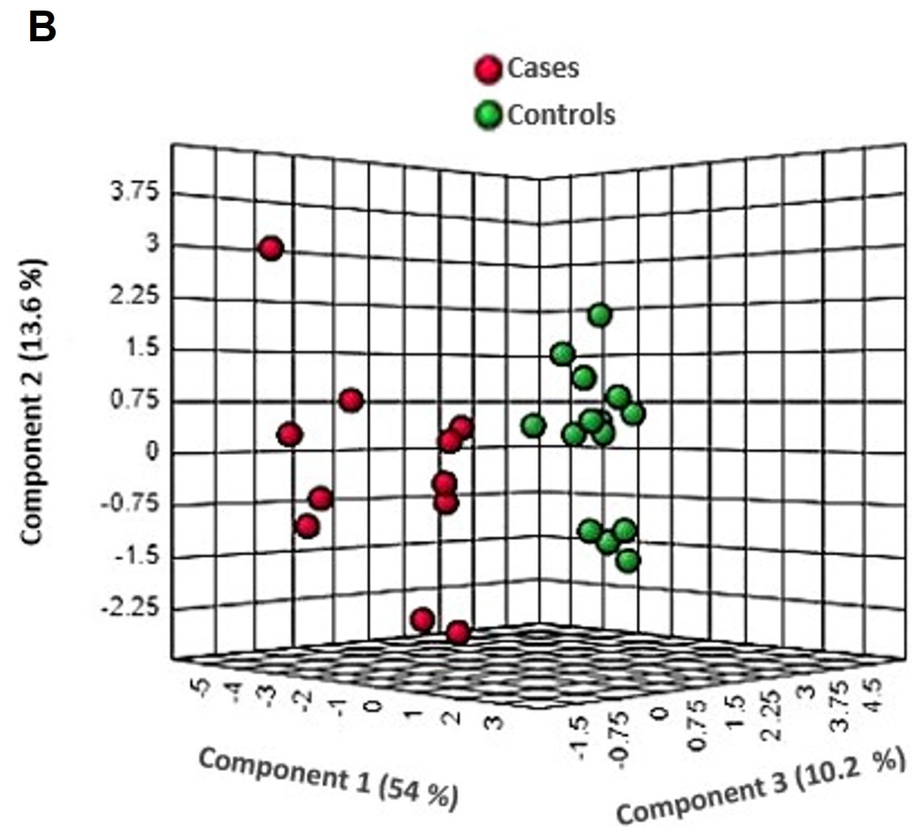
B
Cases
Controls
Component 2 (13.6 %)
3.75
3
2.25
1.5
0.75
0
-0.75
-1.5
-2.25
Component 1 (54 %)
Component 3 (10.2 %)

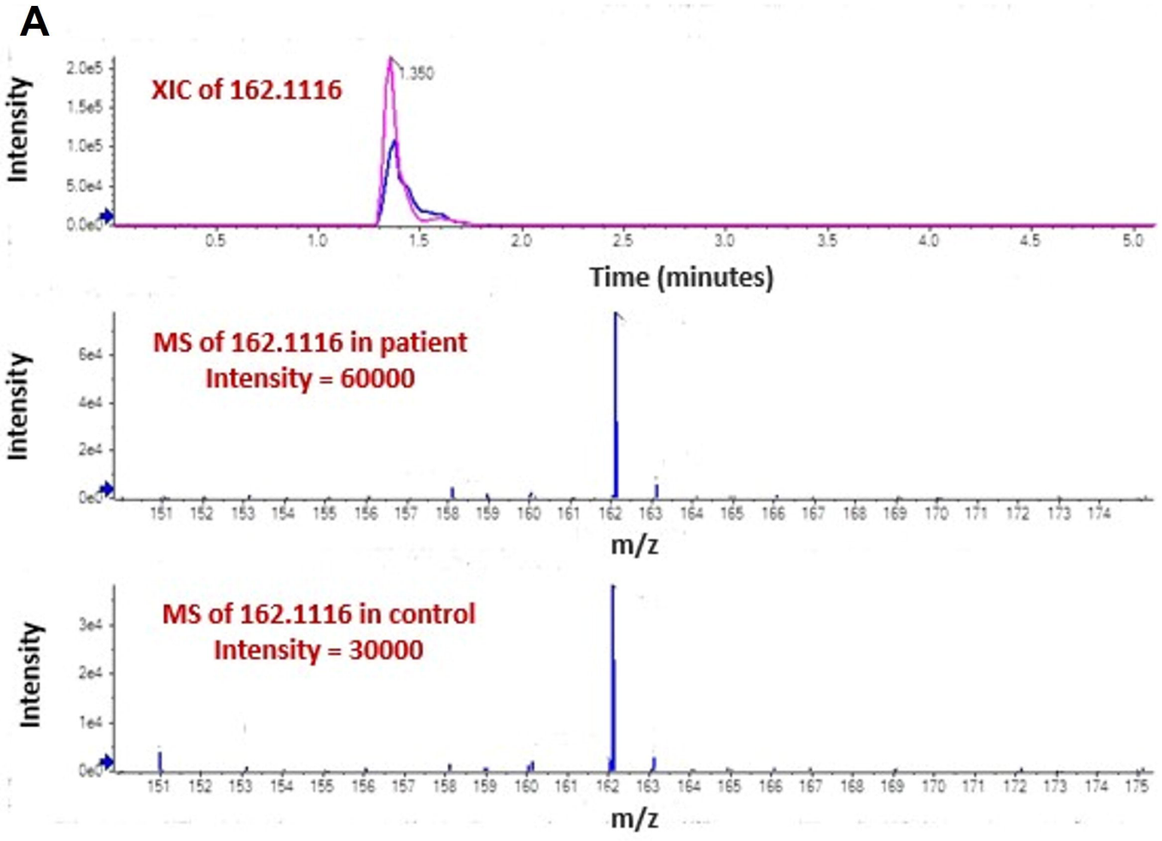
A
XIC of 162.1116
1.350
Intensity
Time (minutes)
MS of 162.1116 in patient
Intensity = 60000
m/z
MS of 162.1116 in control
Intensity = 30000
m/z

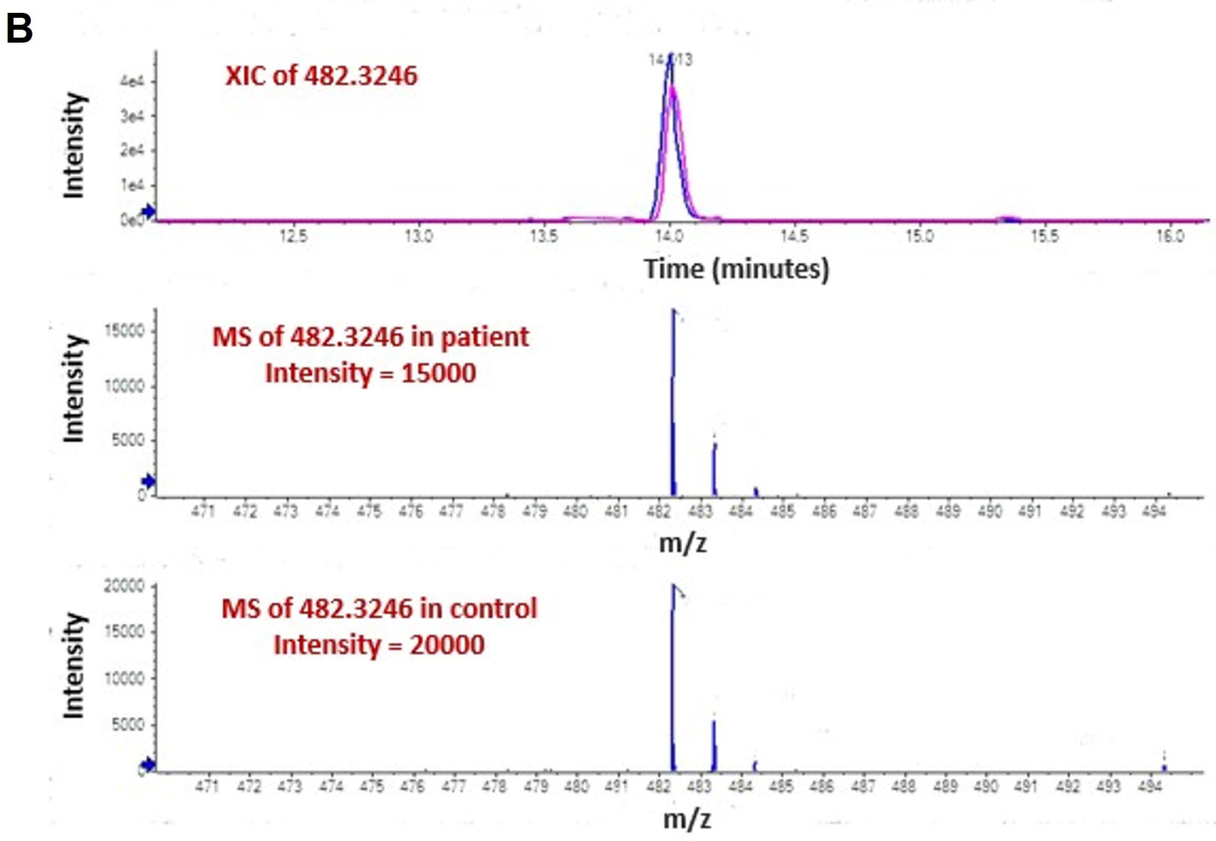
B
XIC of 482.3246
14.013
Intensity
Time (minutes)
MS of 482.3246 in patient
Intensity = 15000
m/z
MS of 482.3246 in control
Intensity = 20000
m/z